Responses to the reviewer' comments:
Subsurface structures of a quick-clay sliding prone area revealed using land-river reflection seismic data and hydrogeological modelling

Silvia Salas-Romero[1*], Alireza Malehmir[1], Ian Snowball[1] and Benoît Dessirier[1,2]

[1]Department of Earth Sciences, Uppsala University, Uppsala, 75236, Sweden
[2]Department of Physical Geography, Stockholm University, Stockholm, 10691, Sweden

Correspondence to: Silvia Salas-Romero (silvia.salas_romero@geo.uu.se)

We thank the anonymous reviewer for the critical and useful comments. We have addressed all the specific comments in our revised manuscript, as detailed below.

(Anonymous Referee #1)
The paper attempts the challenging task of integrating a large collection of geological and geophysical data to derive new insights on landslide formation in quick clays for a specific study area. Primarily using seismic reflection data, the study results in the mapping of the bedrock surface, and an overburden aquifer that may be associated with quick clay formation and landslide activity. However, the paper is poorly organized to the point that the results and their importance are obfuscated. In particular, the authors do not clearly distinguish between established data and interpretation, and the links between the observed data and the process-based conclusions are not effectively demonstrated. The paper would be more impactful if, for example, the authors succinctly identified previously-published data and interpretations, and then demonstrated how new data and insights build on past knowledge to support their objectives. In this fashion, more focus could be placed on the novel aspects of the paper including the hydrogeological modelling, and testing the hypotheses (or supporting the interpretations) of aquifer-driven leaching and sliding mechanism.

(Authors) We thank the reviewer for the comments, which have been useful for improving our manuscript. We have followed the advice and put more emphasis on distinguishing the previous data and our new/current contributions, and relate the last ones to the conclusions.

(Anonymous Referee #1)
Some editing for English is required throughout the paper.

(Authors) A native speaker has gone through the revised version and we hope this problem is fixed. We have taken additional steps to improve the readability and flow of the text.

(Anonymous Referee #1)
p2, L2: Revise sentence.

(Authors) The sentence has been modified.

The new sentence is: ‘The presence of quick clays can only be confirmed using geotechnical site and laboratory investigations enabling estimation of the sensitivity (Rankka et al., 2004). The sensitivity is defined as the ratio of undrained undisturbed to remoulded shear strength.’

(Anonymous Referee #1)
p2, L4: Reference required.

(Authors) A new reference has been added now.

- Karlsson, R. and Hansbo, S. (1989). Soil classification and identification. Byggforskningsrådet Document D8:1989. Stockholm.

(Anonymous Referee #1)
p2: Consider revising/restructuring the introduction to improve focus and logical flow of ideas. Focus switches from geophysics to hydrogeology to site specific conditions all in the same paragraph without any transitions or linking of ideas.

(Authors) We have followed this advice and have restructured the Introduction and ordered the objectives around this, creating a new subsection that clarifies the introductory materials.

(Anonymous Referee #1)
p3: Consider reorganization of material into separate "Intro" and a "Study Area" sections. Geological maps, shot locations, and LiDAR data are not really introductory material. Clearly differentiate between legacy data, and new data. It is not apparent what the new contributions are.

(Authors) As mentioned, we have modified the Introduction and created a new section called Study Area. This new section includes the data that do not belong to the Introduction, such as the geological and topographical data. We also have reworked the text to better describe what legacy data are and what new contributions are.

(Anonymous Referee #1)
p3, L13: The slide is of interest because it is in the middle of the study area?!

(Authors) We have modified the sentence that makes reference to the landslide scar in the study area.

(Anonymous Referee #1)
p.3, L27: Is this the hypothesis being presented? The objective of the paper is not yet clear at this point.

(Authors) No, this is not the hypothesis being presented in this paper. The objectives were listed on p. 3, starting in line 32.

(Anonymous Referee #1)
p.4: If all of these data sets are legacy data sets, they should be well described in the cited references. Much of this information does not seem necessary to support the objectives.

(Authors) All these data are being used within this study for achieving the objectives. We think it is reasonable to reproduce this information so that the article is as complete and as "stand alone" as possible, avoiding too much cross-referencing.

(Anonymous Referee #1)
p.7: Velocity analysis was the "most important step" but receives less discussion than routine operations. How does the time-depth conversion velocity compare to the results of the velocity analysis?

(Authors) Velocity analysis was an important step in the cabled part of line 5–5b, but not the only processing step that improved the quality of the final seismic section (the text has been modified accordingly). The time-depth conversion velocity (1500 m/s) is within the range of velocities picked during the velocity analysis (1100-1600 m/s) and is also consistent with fully saturated clay, which has velocity similar to water. Velocity analysis had to take care of the dip component (dip-velocity dependent stacking velocity) but this is not required for time-to-depth conversion.

(Anonymous Referee #1)
p.7, L32: What is the nature of S1? In particular, does it have finite thickness relative to the wavelength? You refer to it as a layer, an interface and a horizon. How are you picking it? Because it could be interpreted as a compacted top of a reflection package, which seems to be supported by the mag. suc. that increases below S1 and stays high. More discussion of the interpretation logic and reflection facies is necessary. Core?

(Authors) The text has been modified to clarify that S1 represents the top of the coarse-grained layer, i.e. an interface. Our earlier publication in the journal of Landslides and a previous study by Malehmir et al. (2013) already identified S1 and discuss the nature of this layer, using core samples and other evidence.

(Anonymous Referee #1)
p.8, L19: If there is core, how come lithological logs are not part of the analysis?

(Authors) In our previous paper published in Landslides by Salas-Romero et al. (2016) ('Identifying landslide preconditions in Swedish quick clays–insights from integration of surface geophysical, core sample- and downhole property measurements'), grain size distributions are shown for the core samples of the three boreholes (also soil textures are estimated with the natural gamma radiation data). We believe that these results are good enough for describing the core material as they are soils and their appearance is difficult to quantify in a visual inspection (the cores collected in the three boreholes drilled in the study area were visually inspected when samples were collected for the different laboratory measurements).
We use some of the core information from our previous work for supporting the new data, but we prefer not to repeat too much in this manuscript.

(Anonymous Referee #1)
p.9, L32: It looks like a decrease in penetration resistance.

(Authors) We have removed borehole 7073 as the increase in penetration resistance is unclear, but we keep borehole 7075 because it does show an increase in penetration

resistance at the interface S1. It may not be visible at the figure's size but the reference can be checked online.

(Anonymous Referee #1)
p11, L6: The landslide scar is not apparent in Fig.11.

(Authors) We did not mean that the landslide scar is visible in Fig. 11, but that the landslide scar is located in that position and that the deposits located in the river may be related to it.
We have rephrased the sentence and made it clearer to the reader.

(Anonymous Referee #1)
p.11, L11: The paper seems to have been comparing previous studies the whole time.

(Authors) After careful consideration, we decided to remove this subsection.

(Anonymous Referee #1)
p.11, L15: It is unclear how this proposed mechanism works with infiltration "through outcrops and fracture zones" and how this is related to the coarse-grained layer. Consider more development of the hydrogeological conceptual model, and then provide supporting evidence.

(Authors) The hydrological model has been improved and we hope that it now provides sufficient information about the infiltration mechanism.

(Anonymous Referee #1)
p.11, L25: This is well below your quoted resolution. You have not show any frequency spectra, but it is likely well below quarter-wavelength as well.

(Authors) We are aware that our data resolution cannot distinguish such a thin layer. Our intention was to mention that we have checked other borehole data to the north and south of the study area and that the coarse-grained layer can be found in many of them but in some places can be thinner than in our study area.

(Anonymous Referee #1)
p.12, L13: Where are the total sounding data with top and bottom of S1? The nature of S1 and the coarse layer (deposition, thickness, etc.) has not been discussed up to this point.

(Authors) The total sounding data are not included in this manuscript as a lot of information is already present in it. Nevertheless, we provide references about where to find this material, available for any person providing the area information and borehole id.
We discussed largely about the nature of the coarse-grained layer in our paper published in Landslides (reference included in the text). Thus, we do not think it is necessary to discuss it again.

(Anonymous Referee #1)
p.12, L13: Where are the data that go into this most important interpolation? How are you handling the multiple interpreted faults?

(Authors) The boreholes used in the interpolation are now included in a new figure that shows the surface contours. The LiDAR data are shown partially in Fig. 2b. The interpreted faults have not been used for the interpolation of the elevation surfaces.

(Anonymous Referee #1)
p.13, L13: There are more boreholes in Fig.2b than in Fig.14. Need to distinguish water wells from other holes.

(Authors) We have improved the maps and clarified this information distinguishing between the wells used in the hydrological modelling and the others in Fig. 2 and in the new figure showing the surface contours, as mentioned before.

(Anonymous Referee #1)
p.13, L14: It is hard to tell from the figure, but it appears that 3 of 7 boreholes in the model domain (excluding the southern holes) are not fit by the model. This is a lot, and is attributed to "only one measurement" but these holes have not been distinguished from any of the other holes (do they have two measurements?) and the possibility of the model simply being wrong needs to be addressed. Consider presenting and discussing water well data.

(Authors) We provide a table with information about the pore pressure and well data and sort them by depths near the estimated coarse-grained layer (lower aquifer) versus shallower measurements in the fissured near surface clay (upper aquifer). With this distinction in place our simple model manages to approach the former type of values with an RMSE of 0.5 m.

(Anonymous Referee #1)
p.13, L32: This needs to be explained.

(Authors) We have intensively reworked and extended that paragraph to make it clearer to the reader.

(Anonymous Referee #1)
p.14, L5: Explain this. You have "calibrated" the recharge area and the recharge transmissivity which will have a direct trade-off with the required recharge. The modelling requires some sensitivity analysis.

(Authors) A new automated calibration procedure gave better estimates of the optimal values and a better understanding of the model near that minimum (an updated figure was prepared). As can be understood, the two parameters can partially compensate for each other, which leaves some uncertainty in their estimate. Hydraulic tests and/or tracer tests would be required to improve the estimates of the model parameters or to elaborate on the model structure.
This single layer hydrological model was built almost as a back-of-the-envelope scoping calculation and will not bring positive proof of the validity of the leaching assumption as the cause of quick-clay formation. The intention was to provide a quick plausibility check for this area.

(Anonymous Referee #1)

p.14, L8: What data?

(Authors) We rephrased this sentence to make it clearer. The statement is about the pore pressure data.

(Anonymous Referee #1)
p.14, L17: Groundwater velocity of 0.00015m/s or ~13m/day is very fast.

(Authors) We agree with the reviewer. This velocity obviously shows some limitations of the simple hydrological model that isolate the coarse-grained layer.

(Anonymous Referee #1)
p.14: Consider showing and analyzing the mag data with the rest of the data in the data section as opposed to in the discussion section.

(Authors) We have considered it and we still believe that the magnetic data are better discussed in the Discussion, in the subsection about the morphology of the Göta River valley. The data in the Results section are subsurface data describing the subsurface structures, whereas the magnetic data are superficial data.

(Anonymous Referee #1)
p15, L21: Should be easy enough to test with a multivariate regression of mag, T and depth - or some combined variable of T and depth.

(Authors) We thank the reviewer for this useful advice. We tried different tests for comparing the data but most of them were not conclusive. There are a lot of data, and as indicated in the manuscript there are still some anomalies that may be artefacts, that made difficult the comparison between the residual magnetic anomaly, T and depth data. From selected areas what we observed was that shallower depth to the top of the coarse-grained layer and its increased thickness are correlated with high values of the residual magnetic anomaly, thus their effect is difficult to observe because they obscure to each other. The shallower depth to the top of bedrock is also correlated with high values of the residual anomaly, but this is distinguishable from the effect caused by the other two variables. We now include this information in the text and new figures.

(Anonymous Referee #1)
p.17: In my opinion, many of the conclusions from L16 down (and in the abstract) remain conjecture. The catchment area is prescribed without validation, it is not clearly demonstrated that there is aquifer-driven leaching, or that the coarse layer is a sliding surface, and the nature of the mag. anomaly is an interpretation.

(Authors) The conclusions have been modified in order to add the new information obtained after this revision.

(Anonymous Referee #1)
Fig.1: Demonstrate value of this figure.

(Authors) We believe that it is interesting to show the potential for destruction of this type of landslides near the same river in an area very close to the south of our study

area. The current risk of landslides is medium-high in the study area, so we think that the picture is illustrative of a possible scenario.

(Anonymous Referee #1)
Fig.2: Shorten caption. Do not repeat what is stated in the text or what is evident from the figure (such as the legend). Improve figure clarity. Much of the text and symbols on the map are not easily legible.

(Authors) We followed this advice, and shortened the caption and improved the figure clarity.

(Anonymous Referee #1)
Figs.3&4: Remove repetitive material from captions.

(Authors) The captions have been shortened.

(Anonymous Referee #1)
Figs.5&6: The captions are far too long and complicated. The borehole logs require scales and labels (other figures also).

(Authors) The captions have been shortened. We do not think that we require scales for the borehole logs. Precisely, we included close-ups for each borehole (with labels) in every figure for helping to visualize them. The maximum and minimum values for every log are included in the caption of the figure. We believe that adding scales to these figures will worsen their clarity. The same information and more details can be found in our previous work published in Landslides and in the SGI website.

(Anonymous Referee #1)
Fig.12: While visually impressive, perspective images are not good for evaluating interpolated surfaces, particular with respect to potential bias introduced by spatially non-uniform data such as sparse boreholes combined with dense points along seismic lines. Contour plots should be used for analysis. What about coarse layer thickness?

(Authors) We followed this advice and added a new figure that shows the contour plots for the elevation surfaces. The perspective images are now included in the supplementary material for not increasing the manuscript length. We prefer to keep the perspective images because they give a good perspective of the relationship between the surfaces, the river, and possible fault zones.
The coarse-grained layer thickness is an estimation that may include more uncertainties than the delineation of the top of the layer. Figure 14b (transmissivity) shows essentially the layer thickness as T=K*thickness, K=const.

(Anonymous Referee #1)
Fig.13: b and c add nothing.

(Authors) These figures have been removed.

(Anonymous Referee #1)
Table 2: For all but the LiDAR perhaps, these values are nominal resolutions, and the spatial sampling interval is not indicative of the resolution.

(Authors) We agree with the reviewer and we have changed the text accordingly.

Responses to the reviewer' comments:
Subsurface structures of a quick-clay sliding prone area revealed using land-river reflection seismic data and hydrogeological modelling

Silvia Salas-Romero[1*], Alireza Malehmir[1], Ian Snowball[1] and Benoît Dessirier[1,2]

[1]Department of Earth Sciences, Uppsala University, Uppsala, 75236, Sweden
[2]Department of Physical Geography, Stockholm University, Stockholm, 10691, Sweden

Correspondence to: Silvia Salas-Romero (silvia.salas_romero@geo.uu.se)

We thank A. Booth for the critical and useful comments. We have addressed all the specific comments in our revised manuscript, as detailed below.

(A. Booth Referee #2)
a.d.booth@leeds.ac.uk
This is an ambitious paper that shows the strengths of combining multiple data sources together. As the authors point out in the introduction, the analysis is highly multi-disciplinary and multi-methodological, and the hydrological modelling draws on a diverse set of data. Having less expertise in hydrological modelling, most of my comments pertain to the treatment of the geophysical data and the general format of the paper.

We thank the reviewer for his comments, which have been very useful for improving our manuscript. We hope the general format of the manuscript (length and structure) is improved after this revision.

(A. Booth Referee #2)
a) At times, it seems a little lengthy. An aspect of this is the length of some of the paragraphs (Section 4.1, for example, is a monster which spans Pages 8 and 9!); break these up a bit to improve the appreciation of your process.

(Authors) We agree with the reviewer and have reworked different sections and moved figures to the supplementary material for improving the readability.

(A. Booth Referee #2)
b) Sometimes the interpretation of the seismic data is also over-long, but also over-interpreted. I list some specific examples below (Points 13-16), but the key point is that not all of the seismic observations appear to have significance in the model – so I think you should restrict the discussion of the interpretation to the most relevant parameters. A full interpretation could go into supplementary material, although (see below) I'd suggest that some of this is over-interpreted anyway.

(Authors) We followed this advice and reduced the interpretation section. Some of the figures are now included in the supplementary material.

(A. Booth Referee #2)
With such streamlining, the objectives of your paper will be more understandable and

its significance therefore more appreciable.

(Authors) We thank for the comments and hope that the objectives of the manuscript are now clearer.

(A. Booth Referee #2)
Title. This indicates that you reveal subsurface structures with modelling, but I'm not sure this is what you mean. Presumably, the structures you image in the geophysical data help constrain the model? A title like "Hydrological modelling of a quick-clay vulnerable area, constrained with geophysical data" would be more informative?

(Authors) We thank the reviewer for the suggestion. We agree to change the title to 'Subsurface characterization of a quick-clay vulnerable area using near-surface geophysics and hydrological modelling'.

(A. Booth Referee #2)
Abstract. For all the numerical analysis in your paper, the abstract contains no numbers. Can you add some in? e.g., some highlights from the geophysical dataset, and some of the hydrological parameters you use and model?

(Authors) We have added some numerical information to the abstract.

(A. Booth Referee #2)
P1L24: "sensitive" – to what? Makes it sound a bit like they are emotional!

(Authors) This type of clays is usually described using this geotechnical terminology.

(A. Booth Referee #2)
P2L4: Explain the terminology "sensitivity higher than 50"... Is there a unit or a reference system here?

(Authors) The definition of sensitivity is given in this page in line 3. It is the ratio of the undrained undisturbed shear strength to the remoulded shear strength, thus there is no unit.

(A. Booth Referee #2)
P2L7: Surely there's no need to separate "geotechnics, geophysics or geology" out? Aren't they're all "geoscience"?

(Authors) We agree with the reviewer and have modified the sentence for using only the geoscience term.

(A. Booth Referee #2)
Section 2.1 (and throughout): You variously refer to your seismic lines by number, or by the source acquisition method. I found this very confusing, trying to remember what method was used on what line, and would prefer that you stick to the numerical reference throughout. The table usefully informs what source was used anyway.

(Authors) We checked the text and kept the numerical reference when mentioning the seismic lines. Nevertheless, in section 2.1 now 3.1, when the seismic lines are

mentioned are referred by the number and not by the source acquisition method. The mention to the source acquisition method is just an explanation of the acquisition for each line.

(A. Booth Referee #2)
P5L25: No need to say “reflected sound waves”: if they are transmitted as sound waves, they’ll come back as sound waves!

(Authors) The sentence has been modified.

(A. Booth Referee #2)
P6L16: What velocity from the 800-4000 m/s range did you settle on? It doesn’t seem to be listed anywhere.

(Authors) For lines 2–2b, 6 and 7 we used 1400 m/s in the first 150 m depth and 1800 m/s from 150 m depth to the end of the section. So the velocity changed gradually within this range. This information has been added to the text for these lines, and also for the wireless part in line 5–5b (1300 m/s in the first 75 m depth and 3100 m/s from 75 m depth to the end of the profile).

(A. Booth Referee #2)
P7L3: Why the different mute definition for the wireless data?

(Authors) We used a different mute function for the wireless data than for the cabled data because the first option (top mute filter based on the picked first breaks) did not work so well as for the other lines and the cabled part of line 5–5b. Then we tested the surgical mute which worked better for the wireless data.

(A. Booth Referee #2)
P7L23: What is this absolute value of error with respect to? Give it as a fraction of the typical target depth?

(Authors) We modified the sentence and now it is: ‘This value was justified based on the available borehole data for depth calibration. An error on the order of 1-3 m depth can still be expected, which corresponds to e.g. a 1.3-4 % error for a target depth of 75 m’.

(A. Booth Referee #2)
P7L25: To help with the interpretation, it might be worth tabulating the expected response of the different geologies you interpret in each geophysical dataset. Even just listing the range of seismic velocities and resistivities you might expect would help your data description.

(Authors) We thank the reviewer for this interesting suggestion. A table listing seismic velocities and resistivities for every material has been added to the manuscript.

(A. Booth Referee #2)
P8L5: Are you implying that the borehole is 0.02 m, or 0.02 *km* away from the seismic line? If it really is 0.02 m, then it hardly seems worth reporting this, and you could just say that the borehole lies on the seismic line.

(Authors) We modified the text and now we include the sentence 'the borehole lies on the line'.

(A. Booth Referee #2)
P8L7: The interpreted faults are not really clear, and it seems an over-interpretation particularly since refraction static corrections were not applied. Could near-surface anomalies be the origin of the discontinuities and misalignments that you claim? In any case are the faults and damage zones critical to your model? It seems to me that you could be much more tentative in interpreting them, without damaging any parameter in your model.

(Authors) We agree with the reviewer; the discontinuous reflectivity might be related to near-surface anomalies. For avoiding over-interpretation of the seismic data, we re-evaluated all the sections and removed F features where no geological evidence or other evidence was clear.

(A. Booth Referee #2)
P8L8: You don't get a lot of reliable ray coverage in the refraction tomography to really talk about the velocities below reflection B1. I agree that your velocities above this horizon are likely reliable, and you do point out that they have velocities consistent with coarse-grained, saturated sediment. However, in general, I find the resistivity data (Figure 5d, Figure 6e) to provide the much more compelling evidence of a bedrock underburden.

(Authors) We reworked the text for making clearer the information given by the P-wave refraction tomography velocities in lines 2–2b and 5–5b.

(A. Booth Referee #2)
P9L2: On what grounds do you interpret a kinematic response from the seismic data? You see dipping horizons, but I don't see how you can say that this represents a slip surface.

(Authors) We interpreted that the sediments seem disturbed below the landslide scar, apparently moving towards the river (we have modified the sentence). It is only an interpretation; we do not specify that there is a slip surface.

(A. Booth Referee #2)
P9L6: I would suggest that it is beyond the capability of travel-time inversion to resolve boulders, as you claim here. I might expect that they could appear as diffractions in the seismic section, or high-resistivity anomalies, but I don't believe that the tomography would be sensitive to them. Furthermore, this over-interpretation doesn't actually appear to influence any parameterisation of your model, so the paper wouldn't be damaged if you said that your tomography has some unexplained velocity artefacts.

(Authors) We followed the reviewer's advice and modified the text accordingly.

(A. Booth Referee #2)
P11L20: You suggest that the seismic data shows a higher-resolution delineation of the bedrock/sediment contact, but you wouldn't be able to make this interpretation if it

wasn't for the sum total of your datasets! It therefore seems unnecessary to make this assertion when you draw on inferences from all of your data – it doesn't matter which is best! Indeed, this whole section could be considered for removal as it's not clear to me that you are presenting a different hypothesis to one that has been previously postulated. It will always be the case that the use of multiple data sources leads to an improved interpretation.

(Authors) We have reworked this part of the Discussion and removed several parts as the reviewer suggests.

(A. Booth Referee #2)
In the interpretation of Figure 9, you correctly point out in the main text that you are prone to mistaking multiples for genuine reflections. You appear to avoid multiples, except (potentially) for the interpretation between ~800-2500 m in Figure 9b. Can you be sure that this hasn't been misinterpreted? Also, the inset figures here add very little: the data look very fuzzy, so much so that the logs don't appear to correlate with anything at all.

(Authors) After careful consideration we removed this channel from the interpretation. We removed the inset figures too.

(A. Booth Referee #2)
There are potentially too many figures in the paper, and 12 and 13 could be ear-marked for removal as they're not very clear partly because of the limited quality of the seismic data. Could they be moved into supplementary material instead? Equally, once the interpretation is streamlined, I don't think that all the seismic lines need to be included.

(Authors) We followed this advice and now figures 12 and 13 are included the supplementary materials. We have also moved the figures corresponding to lines 6 and 7, and the single-channel river seismic data to the supplementary material.

(A. Booth Referee #2)
Some figure captions need to be reduced in length, typically those relating to the seismic lines (Figures 5,6,8).

(Authors) The length of the captions has been reduced.

Subsurface characterization of a quick-clay vulnerable area using near-surface geophysics and hydrological modelling

Silvia Salas-Romero[1], Alireza Malehmir[1], Ian Snowball[1], and Benoît Dessirier[1,2]

[1]Department of Earth Sciences, Uppsala University, Uppsala, 75236, Sweden
[2]Department of Physical Geography, Stockholm University, Stockholm, 10691, Sweden

Correspondence to: Silvia Salas-Romero (silvia.salas_romero@geo.uu.se)

Abstract. Quick-clay landslides are common geohazards in Nordic countries and Canada. The presence of potential quick clays is confirmed using geotechnical investigations, but near-surface geophysical methods, such as seismic and resistivity surveys, can also help identifying coarse-grained materials associated to the development of quick clays. We present the results of reflection seismic investigations on land and in part of the Göta River in Sweden, along which many quick-clay landslide scars exist. This is the first time that such a large-scale reflection seismic investigation has been carried out to study the subsurface structures associated with quick-clay landslides. The results also show a reasonable correlation with radio magnetotelluric and traveltime tomography models of the subsurface. Other ground geophysical data such as high magnetic values suggest a positive correlation with an increased thickness of the coarse-grained layer, and shallower depths to the top of bedrock and top of the coarse-grained layer. The morphology of the river bottom and riverbanks, as e.g. subaquatic landslide deposits, is shown by side-scan sonar and bathymetric data. Undulating bedrock, covered by subhorizontal sedimentary glacial and postglacial deposits is clearly revealed. An extensive coarse-grained layer (P-wave velocity mostly between 1500 and 2500 m/s, and resistivity approximately from 80 to 100 Ωm) exists within the sediments and is interpreted and modelled in a regional context. Several fracture zones are identified within the bedrock. Hydrological modelling of the coarse-grained layer confirms its potential for transporting fresh water infiltrated in fractures and nearby outcrops located in the central part of the study area. The modelled groundwater flow in this layer promotes leaching of marine salts from the overlying clays by seasonal in/outflow cycles and/or diffusion, which contributes to the formation of potential quick clays.

1 Introduction

Quick clays are sensitive glacial and postglacial sediments, mostly deposited in a shallow-water marine environment, whose structure can collapse and liquefy if disturbed (Osterman, 1963; Torrance, 2012). These sediments were deposited in the last deglaciation and early postglacial, and subsequently isostatically raised above sea level (Torrance, 2012). Due to the infiltration of meteoric waters, mineral salts were leached out, which changed the salinity of the pore water and altered their soil properties (Rosenqvist, 1953). Leaching of salts is important in the development of the characteristic quickness behaviour (Rosenqvist, 1946; Torrance, 2012), but there are other factors that influence the formation of quick clays, such as

Deleted: Subsurface structures of a quick-clay sliding prone area revealed using land-river reflection seismic data and hydrogeological modelling

Deleted: the
Formatted: Not Highlight
Formatted: Not Highlight
Formatted: Not Highlight
Formatted: Not Highlight
Formatted: Not Highlight
Formatted: Not Highlight
Deleted: in the
Deleted: ary sequence
Deleted: Individual fractures and
Deleted: f
Deleted: and sediments
Formatted: Not Highlight
Deleted: the coarse-grained
Deleted: slow infiltration
Formatted: Not Highlight
Deleted: helps
Deleted: in
Deleted: Magnetic data show coarse-grained materials at the landslide scar located in the study area, which may have acted as a sliding surface together with quick clays.

the presence of dispersing agents and pH level (Salas-Romero et al., 2016; Torrance, 2012). The presence of quick clays can only be confirmed using geotechnical site and laboratory investigations enabling estimation of the sensitivity (Rankka et al., 2004). The sensitivity is defined as the ratio of undrained undisturbed to remoulded shear strength. In Sweden, where this work is focused, quick clays are defined as clays with sensitivity higher than 50 and remoulded shear strength of less than 0.4 kPa (Karlsson and Hansbo, 1989).

Quick-clay landslides are common in northern countries such as Sweden, Norway and Canada. They are also known world-wide due to catastrophes such as in Rissa (Gregersen, 1981), Tuve (Larsson and Jansson, 1982), and Saint-Jude (Locat et al., 2017), and they have been studied in different fields of geoscience (Dahlin et al., 2013; Lundström et al., 2009; Salas-Romero et al., 2016; Sauvin et al., 2014; Solberg et al., 2016; Wang et al., 2016). In order to define areas susceptible to quick-clay landslides in Sweden, Rankka et al. (2004) reviewed a number of geological and geohydrological prerequisites for the formation of quick clay. This list includes; glaciomarine sediments, thin clay deposits, underlying coarse-grained layers, peaks in the bedrock surface that retain accumulating groundwater, artesian groundwater pressure, highly permeable layers within the clay deposits, height above sea level, organic soils, a large catchment area, and infiltration from more than one direction. Triggering of quick-clay landslides is influenced by natural conditions (heavy rainfall, high-low water flow along the river, river erosion or variation of the groundwater level) and by human activities (constructions or loading/unloading works) (Thakur et al., 2014). With a minimal slope angle and a place to flow to, any mechanism that increases stress on the quick clays or reduces their strength may trigger a landslide. In Sweden, the model scenarios for climate change over the next hundred years predict warmer and wetter conditions (Swedish Government Official Reports, 2007), which means more precipitation in the west of the country, more runoff water and higher river discharge, increasing the likelihood of landslides in areas that are already prone to them. More variability in river level, as predicted by the climate studies (Swedish Government Official Reports, 2007), may destabilize some slopes along the shores, causing new landslides.

The Göta River valley, which is located in southwest Sweden, hosts many landslide scars, most of which are quick-clay related (Swedish Geotechnical Institute–SGI, 2012a). The valley is filled with thick marine postglacial deposits that overlie undulating bedrock (SGI, 2012a). The Göta River is one of the longest rivers in Sweden (93 km long), the source of drinking water for more than 700,000 people, a transport route, and is the main outflow of the country's largest lake, Vänern (SGI, 2012a). One or more large landslides could dam the river, affecting river-based transportation and have economic and social consequences. In June of 1957 a landslide took place at the sulfite factory located next to the Göta River (in the southern part of the municipality of Lilla Edet). This landslide, one of the biggest to have been observed in Sweden, caused a lot of structural damage (Fig. 1) and the loss of three lives. The landslide propagated backwards in a retrogressive manner and along the riverbank, transporting large amounts of materials into the river, triggering a wave of 5 to 8 m height and covering around 32 hectares (Hultén, 2006; Odenstad, 1958). It has been suggested that the landslide was triggered by the infiltration of sulfite liquor and other chemicals into the ground, which reduced the clay shear strength, in combination with other factors such as the erosion at the riverbank and the presence of quick clay (Odenstad, 1958).

Deleted: 5
Deleted: , estimating
Deleted: t
Deleted: , i.e. is equal to
Deleted: world
Deleted: from
Deleted: like geotechnics, geophysics or geology
Deleted: 5
Deleted:
Deleted: in nature
Deleted: d
Moved (insertion) [2]
Deleted: T
Deleted: sent
Deleted: a
Deleted: Sweden
Deleted:
Deleted:

This study is based on a joint interpretation of multidisciplinary datasets for testing that an area close to the centre of Lilla Edet is susceptible to quick-clay landslides using the prerequisites described by Rankka et al. (2004), focusing on building a hydrogeological model that may represent the study area. The detailed objectives are (i) 3D geological/geophysical modelling of the larger-scale subsurface structures overlying and existing within bedrock – like possible fracture zones, (ii) understanding the role of an identified coarse-grained layer and its spatial relationship with the bedrock surface that may improve the hazard assessment, (iii) hydrological modelling of the groundwater within the coarse-grained layer to better understand the development of quick clays in the study area, and (iv) investigating the riverbanks of the Göta River, its bed and mass-movement deposits. Reflection seismic (both legacy and new sets of seismic profiles acquired within this study), P-wave refraction tomography (mainly from Wang et al. (2016) but for the new profiles performed in this study), and resistivity models (Bastani et al., 2017; Wang et al., 2016) are correlated with borehole data (Branschens Geotekniska Arkiv–BGA, 2018; Salas-Romero et al., 2016) for the identification of different types of clays, coarse-grained materials and bedrock. Using the interpreted seismic sections together with total sounding (BGA, 2018) and high-resolution LiDAR data (© Lantmäteriet), elevation surfaces from the top of bedrock and top and bottom of the coarse-grained layer are modelled. This study demonstrates not only that this layer covers a larger area than initially thought (earlier studies showed the local extension of this layer), but also confirms its hydrological potential as a transport path for infiltrating fresh water from nearby outcrops and fractures. Surface magnetic data serve for illustrating that the coarse-grained layer together with quick clays may have acted as sliding surface at a the landslide scar located within the survey area. Other datasets, such as side-scan sonar and bathymetry, are also analysed to investigate the riverbed and their influence on the development of quick-clay landslides. This work provides a good example of the integration of a large amount of different types of data for the study of an area prone to quick-clay landslides.

Moved (insertion) [1]
Deleted: research
Formatted: Font:10 pt, English (UK)
Deleted:
Deleted: for
Deleted: the
Deleted: ,
Deleted: 5
Deleted: shows
Deleted: probably
Deleted: M
Deleted: surface
Deleted: surface
Deleted: .

2 Study area

Formatted: Heading 2, Left, Space Before: 24 pt, Line spacing: single

The work presented in this paper is a continuation of previous studies conducted in an area prone to quick-clay landslides in southwest Sweden in 2011 and 2013 (Malehmir et al., 2013a, Salas-Romero et al., 2016). The study area is within the municipality of Lilla Edet in a region called Fråstad, which the Göta River crosses. Lilla Edet has around 14,000 inhabitants (Lilla Edets Kommun, 2017), and is located approximately 8 km south of this area, on the eastern side of the river. The geology of the study area consists mostly of gentle reliefs of glacial and postglacial deposits such as clay, silt and sand, with some granite to granodiorite bedrock outcrops (© Geological Survey of Sweden–SGU, Fig. 2a). Along the shorelines, landslide scars can be found. Precisely at the survey site several landslide scars are visible along both sides of the river, one of them located in the middle of the survey area (Fig. 2a–b). A net of morphological lineaments, mostly fracture zones, covers most of the area represented in Fig. 2a. Among these lineaments, one of the prominent ones follows the river profile and another one has an E-W direction. It is known that the bedrock in the Göta River valley has an extended system of cracks, with a fault zone that follows the river channel (SGI, 2012b). Figure 2b shows high-resolution LiDAR data (©

Deleted: done
Deleted: 5
Deleted: crossed by
Deleted: at
Deleted: being of particular interest due to its
Deleted: ion

Lantmäteriet) ranging from 7 to 97 m elevation. Two of the seismic profiles acquired in this study, lines 6 and 7, are located in an area with lower elevation compared to the rest of the land seismic lines. In this area a large landslide scar is visible (Fig. 2a–b) and shows a horst and graben pattern, classifying this landslide as spread type (Demers et al., 2107). Previous studies included P- and S-wave reflection and refraction surveys, potential fields, controlled-source tensor (CSTMT) and RMT, electric resistivity tomography (ERT), and ground-penetrating radar (GPR). In 2013 three boreholes (BH1 to BH3 in Fig. 2a–b) were made in the study area primarily to ground truth geophysical interpretations but also to collect undisturbed core samples for laboratory measurements. Geophysical, geotechnical and borehole data showed that a coarse-grained layer underlies leached clays (potential quick clays) and quick clays in some places within the study area. The studies suggested that this layer plays a role in leaching the marine salts from the overlying clays and speeds up the formation of quick clays. Some geotechnical investigations (Löfroth et al., 2011) showed that an increased thickness of the coarse-grained layer is correlated to an increased thickness of the quick clays. The sediments above the coarse-grained layer are intercalating layers of silt and clay, and below they are mostly marine clays that extend down to bedrock. The studies also suggested the eastern part of the study area has higher proportion of leached clays than the western part.

3 Data acquisition

3.1 Land reflection seismic

Four land reflection seismic profiles were acquired (this study) during two weeks in 2013 (lines 2b, 5b, 6 and 7 in Fig. 2a–b) totalling a length of approximately 3.8 km, aiming to complement existing reflection seismic data (Lundberg et al., 2014; Malehmir et al., 2013a, 2013b) and to obtain an overall understanding of the larger-scale structures. The new lines extend the study area along the N-S direction as line 5b crossed to the northern side of the river. Table 1 compiles the main acquisition parameters. In three of the lines, 2b, 6 and 7, the geophone and shot spacing were the same (4 m), while in the longest line, 5b, they were different. In the southern part of line 5b cabled geophones of 28 Hz were used every 4 m, and in the northern part wireless stations were deployed every 10 m, alternating single-component (1C) receivers of 10 Hz and three-component (3C) broadband digital MEMs (micro-electro mechanical systems) sensors. Due to the great length of line 5b (~2300 m), dynamite was used as the source energy and fired at every 20 m in order to obtain high-quality data. In line 2b an accelerated weight drop was used, and in lines 6 and 7 a sledgehammer was the main seismic source because the accelerated weight drop experienced technical problems. At the beginning and at the end of lines 6 and 7, extra shots were made using dynamite. These two lines were connected to each other during the survey, which allowed simultaneous data acquisition along both lines. Due to the large distance between them (~300 m) the initial idea of a joint 3D first-break tomography to resolve the bedrock surface was not possible, nevertheless individual results were obtained for each line (Wang et al., 2016). The acquisition system was Sercel 428^{TM}, and the survey coordinates were obtained using a differential global positioning system (DGPS) with high-precision geodetic data. The ranges of lateral and vertical nominal resolutions for this method are shown

Deleted: A couple
Deleted: survey
Deleted: At this position
Deleted: that
Formatted: Level 1
Deleted: T
Deleted: when the
Deleted: thicker,
Deleted: the
Deleted: is also larger
Deleted: .
Moved up [1]: This research is based on a joint interpretation of multidisciplinary datasets for (i) 3D geological/geophysical modelling of the larger-scale subsurface structures overlying and existing within bedrock – like possible fracture zones, (ii) understanding the role of the identified coarse-grained layer and its spatial relationship with the bedrock surface that may improve the hazard assessment, (iii) hydrological modelling of the groundwater within the coarse-grained layer to better understand the development of quick clays in the study area, and (iv) investigating the riverbanks of the Göta River, its bed and mass-movement deposits. Reflection seismic, P-wave refraction tomography (Wang et al., 2016), and resistivity models (Bastani et al., 2017; Wang et al., 2016) are correlated with borehole data (Branschens Geotekniska Arkiv–BGA, 2018; Salas-Romero et al., 2015) for the identification of different types of clays, coarse-grained materials and bedrock. Using the interpreted seismic sections together with total sounding (BGA, 2018) and high-resolution LiDAR data (© Lantmäteriet), elevation surfaces from the top of bedrock and top and bottom of the coarse-grained layer are modelled. This study shows not only that this layer probably covers a larger area than initially thought (earlier studies showed the local extension of this layer), but also confirms its hydrological potential as a transport path for infiltrating fresh water from nearby outcrops and fractures. Magnetic surface data serve for illustrating that the coarse-grained layer together with quick clays may have acted as sliding surface at the landslide scar located within the survey area. Other surface data, such as side-scan sonar and bathymetry, are also analysed to investigate the riverbed and their influence on the development of quick-clay landslides. This work provides a good example of the integration of a large amount of different types of data for the study of an area prone to quick-clay landslides.
Deleted: 2
Deleted: 2
Deleted: totalling
Deleted:
Deleted:
Deleted: is

in Table 2. The shown lateral nominal resolution for the reflection seismic data has been obtained calculating the first Fresnel zone at 20 m depth.

3.2 River reflection seismic

Reflection seismic data along the Göta River were acquired from the survey vessel SV Ocean Surveyor (property of SGU) in 2000, and were made available as raw shot records. Two types of acquisition were registered: single-channel (3.5 kHz echo sounder) and six-channel (Fig. 2a–c). Both lines have similar length (around 16.9 km) and run parallel, with their initial and final points very close to each other (they are shifted with respect to each other by approximately 11 m). In the single-channel line the receiver and shot positions were the same (the average distance between consecutive points is 3 m). In the six-channel line the distance between the source and the nearest receiver is 6 m (maximum offset is 21 m), the receiver spacing being 3 m. A 10 in^3 sleeve gun was used as source. The frequency range is between 100 and 1000 Hz. Table 2 shows the lateral and vertical nominal resolutions for this method, which have been calculated following the same procedure as in the land reflection seismic data.

3.3 Magnetics

The ground magnetic data were collected by Uppsala University during the field campaign of 2011 (Malehmir et al., 2013a). The purpose of this survey was to delineate the bedrock topography by estimating the changes in the magnetic field generated by the rock magnetism. The total-field magnetic and vertical gradient were measured using a walking mode GPS-mounted magnetometer during five days. During the first three days a N-S direction was followed and during the last two days an almost E-W direction. In total, 17128 points were surveyed (see spatial sampling in Table 2). A base station was used for correcting the diurnal variations and instrumental drift. The position of this base station changed along the five days, with the biggest difference between the first and the rest of the days (around 53 m). The vertical gradient data did not provide convincing results and thus were disregarded for detailed studies.

3.4 Side-scan sonar and bathymetry

The side-scan sonar data on the Göta River were acquired by SGU in 2000, and were available as a 2D georeferenced image file (see Table 2). The system used was a klein of 500 kHz. These data are obtained by transmitting sound waves, which are then reflected from underwater elements, and allow to produce an acoustic image of the materials and morphology of the riverbed (Kaeser et al., 2013). The amplitude values of the image are represented with a grey scale that indicates the strength of the reflectivity and possible density of the materials. Normally, dark areas are considered coarse materials like gravel, and light areas are considered fine materials like clays. The side-scan sonar data cover most of the river shown in Fig. 2a–b, and extending a bit further to the south.

Deleted: , together with the spatial sampling information from other methods used in this work

Deleted: 2

Deleted: ‘

Deleted: ’

Deleted: 2

Deleted: east

Deleted: west

Deleted: 2

Deleted: eceived as reflected sound waves

Marin Miljöanalys AB collected the bathymetric data using multi-beam echo sounding (Kongsberg EM3002-D, 300 kHz) in 2009 under the assignment of SGI (Marin Miljöanalys AB, 2009). The goal was to create a high-resolution topography model of the riverbed. The data were available as a georeferenced file (see nominal resolution in Table 2).

3.5 LiDAR

The LiDAR scan was collected by Lantmäteriet in 2011. The survey was made from a height of 2000 m and the average point density is from 0.5 to 1 points/m^2 (see nominal resolution in Table 2).

4 Reflection seismic processing

Table S1 presents the detailed processing steps for the land and river reflection seismic data. The processing of the land reflection seismic data was similar for lines 2–2b, 6 and 7. The preparation of the data required zero-time correction, vertical stacking of repeated shot records, as well as merging of the new line 2b with the 2011 line 2 (Malehmir et al., 2013b). Removal of first arrivals using a carefully designed top mute filter using picked first breaks and the application of stretch mute (Schmelzbach et al., 2005) helped to enhance the reflections at the shallow parts and avoid misinterpretation of the first arrivals. Refraction static corrections did not give satisfactory results for any of the lines, and they were not applied further. Elevation static corrections were, however, applied using the highest elevation as datum and a velocity of 1500 m/s. As the data still looked noisy and with lower resolution, more preprocessing steps were necessary. Deconvolution before stacking helped in obtaining a reasonably clear seismic section. A series of constant velocity stacks (from 800 to 4000 m/s) was used in order to obtain the most coherent bedrock reflections. For lines 2–2b, 6 and 7 we used 1400 m/s in the first 150 m depth and 1800 m/s from 150 m depth to the end of the section. A post-stack *fk*-filter and surface-consistent residual static corrections were applied for data along lines 6 and 7 for improving the continuity of the reflections. Black et al. (1994) show that the migration process is not really necessary for near-surface seismic imaging applications although it can reduce the noise level. After a series of tests, we eventually concluded that migration did not lead to any improvement because the reflections are mostly subhorizontal or gently dipping.

Figure 3 shows an example of a shot record from line 7 (SH7, see the position in Fig. 2a). Figure 3a presents the raw shot gather with only trace balance applied, and Fig. 3b presents the preprocessed shot gather after elevation static corrections, Wiener deconvolution, band-pass filter, trace editing, removal of first breaks and trace balance. The bedrock reflection, B1, is visible already in the raw data but improved in the preprocessed shot record.

The processing of the land reflection seismic data for line 5–5b was slightly different from the rest of the lines. First, the wireless data needed to be resampled from 1 to 0.5 ms to be consistent with the cabled geophone data. Then, the cabled geophone, 1C and 3C wireless (vertical component) data were merged. Once all the data were joined, a delay of around 1 s between the cabled geophone and the wireless part was observed (the wireless data were shifted up 1 s). With the data zero-time shifted, the next step was to merge them with those from the 2011 line 5 (Malehmir et al., 2013b). As the receiver

Deleted: 2

Deleted: done

Deleted: 3

Deleted: 3

Deleted: main

Deleted: tests

distance was different for the cabled geophone and the wireless parts, it was necessary to process each part separately, applying different geometries for each case (common depth point, CDP, spacing equal to 2 m in the south and 10 m in the north). Before velocity analysis, both processing included elevation static corrections, removal of first arrivals using a top mute filter (surgical mute for the wireless data), band-pass filter, spectral whitening, and *fk*-filter for the wireless data. The high-quality data for line 5–5b allowed a relatively simple processing flow, where the velocity analysis greatly improved the result of the final seismic section (performed at 10-20 m lateral spacing in the southern part; in the northern part constant velocities, from 800 to 4000 m/s, were tested). The velocity analysis of the wireless seismic data revealed that the deeper part of the section needed higher velocities to obtain visually coherent reflections, thus the data were divided in two parts for processing: from 0 to 80 ms (using a velocity of 1300 m/s) and from 80 to 500 ms (using a velocity of 3100 m/s). The post-stack processing included band-pass filter for both types of data (cabled geophone and wireless), and post-stack deconvolution in the case of the wireless data.

Figure 4 shows an example of a shot record along line 5–5b (SH5, see the position in Fig. 2a). Figure 4a is the raw shot gather, and Fig. 4b is the preprocessed shot gather (elevation static corrections, band-pass filter, spectral whitening, trace editing, removal of first breaks and automatic gain control, AGC). In Fig. 4b a number of reflections seem to be revealed; bedrock reflection B1 and a shallower one from the top of the coarse-grained layer S1. The sediments show P-wave velocities ranging from 1000 to 2000 m/s, while bedrock shows velocities much higher than 3000 m/s (Wang et al., 2016). The values are similar to those in line 7 (Fig. 3a), except for the direct wave, which is much slower in that case. It may be related to near surface effects or differences in topography.

The processing of the river reflection seismic data was simpler compared to the land seismic processing (Table 3). In the case of the single-channel data only Wiener deconvolution was applied for removing multiples as much as possible. The six-channel data required the creation of marine geometry according to the receiver and shot positions. A CDP spacing of 1.5 m was used for making the geometry. For the six-channel data more processing steps were necessary, where Wiener and post-stack deconvolution helped to improve the final results.

Land and river reflection seismic data were time to depth converted using a constant velocity of 1500 m/s. This value was justified based on the available borehole data for depth calibration. An error on the order of 1-3 m depth can still be expected, which corresponds to e.g. a 1.3-4 % error for a target depth of 75 m.

5 Results and interpretations

5.1 Land seismic lines

Figure 5a–d shows, from top to bottom, the seismic results for line 2–2b, the interpreted interfaces, i.e. S1 and B1, and the P-wave refraction tomography and RMT resistivity results obtained in earlier studies (Wang et al., 2016). Figure 5b also includes the natural gamma radiation and magnetic susceptibility data from borehole BH1 (distance to the line 13.4 m; Salas-Romero et al., 2016), and the total sounding data from borehole 7065 (the borehole lies on the line; BGA, 2018). S1 is a

Deleted: the most important step was

Deleted: a

Deleted: , although a slight

Deleted: 4

Deleted: 4

Deleted: horizons

Deleted: and structures

Deleted: ,

Deleted: and F

Deleted: 5

subhorizontal interface only identified in the southeastern part of the line; the strong decrease in the gamma log of BH1 and the increase of magnetic susceptibility coincide with this interface. In the northwestern part of the line, next to the river, the S1 reflection is not visible. This interface is the top of the coarse-grained layer previously identified in Salas-Romero et al. (2016). B1, interpreted as the top of bedrock (BH1 reached the top of bedrock, see Salas-Romero et al., 2016), is more irregular and has a higher amplitude reflection than S1. B1 shows a clear undulating morphology, reaching the ground surface at approximately CDP 525, and dipping towards the river in the northwestern side; in borehole 7065 the strong increase in the total sounding curve happens at bedrock depth.

The P-wave refraction tomography results (Fig. 5c) indicate high velocities (>4000 m/s) below B1 in the southeastern side, but poor ray coverage in the northwestern side. The S1 interface shows for the most part higher velocities (1500-3000 m/s) compared to the sediments above and below this interface (mostly below 2000 m/s) in the southeastern part of the line. The resistivity results only cover part of the line (Fig. 5d); above the thin dashed white line, the RMT model is well resolved with high confidence. Wang et al. (2016) estimated the penetration depth (thin dashed white line position) using a method shown by Spies (1989), and the same criterion is followed for the rest of the lines. Low resistivity values (between 3 and 100 Ωm) are observed above B1, and higher values (>100 Ωm) below, with very high at the position closer to the surface (up to 1000 Ωm, some outcrops are close to this location, see Fig. 2b). At the S1 position the values are around 80-100 Ωm, which agrees with the material classification (coarse sediment) presented by Solberg et al. (2012). The values immediately above S1, between 10 and 80 Ωm, may indicate silt or leached clay deposits–potential quick clays (Solberg et al., 2012). Quick clay was identified above the coarse-grained layer during the visual inspections of the core samples of boreholes BH1 to BH3 (Salas-Romero et al., 2016). Table 3 provides information about the general intervals of P-wave velocities and resistivities for each material identified in the study area (based on the results obtained in Salas-Romero et al., 2016).

Figure 6a–e shows the seismic results for line 5–5b, their interpretation, the earlier P-wave refraction tomography and RMT resistivity results (Wang et al., 2016), and the airborne transient electromagnetic (ATEM) resistivity results (Bastani et al., 2017). Figure 6b also includes the natural gamma radiation and magnetic susceptibility data from borehole BH3 (distance to the line 0.23 m; Salas-Romero et al., 2016), and the total sounding data from borehole 7062 (distance to the line 90.3 m; BGA, 2018). Note that the quality of the seismic data is different on each side of the river, due to the lower sampling in the northern side (10 m). Nevertheless, the delineation of S1 and B1 is possible along the whole line. The S1 interface shows continuity along the line, except between CDPs 400 and 480. At these positions S1 is not visible, likely due to lower fold in the seismic data (see fold distribution along line 5–5b in Fig. 6a). Other possibilities cannot be disregarded, e.g. bedrock movement and/or fractures in the bedrock, and/or deposits disturbed by human activities such as excavation works. A fracture (F) can be inferred in the bedrock at around CDP 440 with some diffraction signatures suggesting the presence of a strong bedrock curvature or edge. The biggest changes in the gamma and magnetic susceptibility logs in BH3 and in the total sounding curve in 7062 coincide with the depth of S1. The undulating B1 reaches close to the surface around CDP 500 and dips to the river after this point; no clear bedrock dipping is observed in the opposite northern shore data. Below the

Deleted: layer

Deleted: (distance to the seismic line 13.4 m)

Moved (insertion) [3]

Deleted: the

Deleted: S1

Deleted: a

Moved up [3]: In the northwestern part of the line, next to the river, the S1 reflection is not visible.

Deleted: 5

Deleted: 5

Deleted: (distance to the seismic line 0.02 m)

Deleted: , not showing any important change at the suspected position of S1

Deleted: The discontinuous reflectivity at bedrock level indicates the presence of fractured or disturbed materials (F) in the northwestern side.

Deleted: ,

Deleted: in general,

Deleted: and lower velocities in the overlying sediments (mostly between 350 and 3000 m/s). The top of bedrock is

Deleted: well delineated

Deleted: by high velocities with some exceptions at the extremes of the line, which may be due to the lack of ray coverage

Deleted: horizon

Deleted: layer

Deleted: given in

Deleted: 5

Deleted: 5

Deleted: horizon

Deleted: (a trench runs perpendicular to the line at this position, although neither its width nor its depth seem to be of the same size of the observed anomaly in the seismic data)

Deleted: (distance to the seismic line 0.23 m)

Deleted: (distance to the seismic line 90.3 m)

landslide scar displacement and oblique translation of some reflections are observed; the sediments appear to have moved towards the river. The top of bedrock at the river position may be at a depth of around 100 m.

The P-wave refraction tomography results (Fig. 6c) in the southern side indicate, in general, high velocities (>3000 m/s) below B1 and lower velocities in the overlying sediments (between 300 and 1500 m/s). In the northern side of the line, the tomography results and reflection B1 agree in the northernmost part of the profile, with poor ray coverage below B1. Nevertheless, unexplained velocity artefacts are visible above B1 from the river to CDP 1000. The S1 interface shows higher velocity than the sediments around it in the northern part of the line, which is similar to what is observed in Fig. 5c. In contrast, the southern part of the line does not show any velocity difference at the S1 interface. The RMT resistivity values (Fig. 6d) are mostly high (>100 Ωm) below B1 although the northern side does not have data below the top of bedrock. Above B1, the RMT resistivity values are low (between 1 and 10 Ωm) except along S1, where the values reach >100 Ωm. The values immediately above S1 may indicate leached clay deposits–potential quick clays (Solberg et al., 2012). The ATEM resistivity values (Fig. 6e) do not to delineate the interface B1 as well as the RMT resistivity results in the southern part of the profile, except at the position where the bedrock is closer to the surface. In the northern part of line 5–5b the penetration depth of the ATEM model does not reach the position of B1. In comparison, the ATEM resistivity results seem to delineate the interface S1 between CDPs 500 and 700, and 880 and 1000. Malehmir et al. (2016) interpret a possible fault (low resistivity values sandwiched between high resistivity values identified as bedrock) on the southern shore of the river, between CDPs 730 and 750 approximately at 30 m below sea level.

Figures S1a–c and S2a–d show similar seismic results for lines 6 and 7, their interpretation and the earlier obtained P-wave refraction tomography and RMT resistivity results (Wang et al., 2016). Figure S2b also includes the total sounding data from borehole 7075 (distance to the line 1.6 m; BGA, 2018). B1 is delineated along both lines (Figs. S1b and S2b), showing undulating morphology, approaching to the ground surface in the eastern side and dipping towards the river in the western side. In contrast, the S1 reflection is only delineated between CDPs 100 and 210 in line 7 (Fig. S2b). Borehole 7075 located in the western side of the line shows strong increases in the curves at the S1 interface. In Fig. S1b, between CDPs 100 and 200 from -50 to -100 m elevation, a different reflection pattern (dipping to the east of the line) is present, which may be related to 3D effects caused by the rough bedrock topography. Fractured or disturbed materials (F) are identified in the western side of line 6 (Fig. S1b). The F materials located seem to coincide with a probable fracture zone present in Fig. 2a, which runs parallel to the river profile. The P-wave refraction tomography results (Figs. S1c and S2c) are similar for both lines. The velocities are high in the eastern side (>3000 m/s) below B1 and low in the overlying sediments (approximately between 450 and 2000 m/s). In the western side of the lines the ray coverage is poorer at the depth of B1. The resistivity values in line 7 are high (>100 Ωm) below B1 in the eastern side (Fig. S2d); the western side does not have resistivity results below B1 and only partial results above it. The resistivity values are around 10 to 100 Ωm at shallower depths, except at the S1 position and below it where the values are lower, between 1 and 10 Ωm. In terms of resistivity, these values do not indicate coarse sediments but unleached marine clay deposits (Solberg et al., 2012). Nevertheless, the resistivity model is not well resolved below 10 to 30 m depth along the line.

Deleted: slid

Deleted: high velocities (>3000 m/s)

Deleted: F

Deleted: individual high-velocity anomalies (>4000 m/s) are visible above B1, which may be related to the presence of boulders

Deleted: horizon

Deleted: for line 2–2b

Deleted: the

Deleted: horizon

Deleted: Where there is coincidence, the range of ATEM resistivity values is similar to the range of RMT resistivity values mentioned earlier.

Formatted: Font:10 pt

Deleted: 7

Deleted: s

Deleted: the

Formatted: Font:10 pt

Deleted: In this case only B1 is identified in the seismic section. The bedrock shows undulating morphology,

Deleted: to the west

Deleted: , and reaches the ground surface at the end of the line in the eastern side

Formatted: Font:10 pt

Deleted: B

Deleted: (Fig. 7b),

Deleted: the

Deleted: and also at around CDP 260

Deleted: closer to the river

Deleted: The velocities (Fig. 7c) are, in general, high (>3000 m/s) below the B1 reflector, except between CDPs 150 and 200 where the velocity is high (>3000 m/s) above B1. „

54

Deleted: 8c

Deleted: to the ones shown in

Deleted: e 6 (Fig. 7c)

Deleted: The tomography results do not show any velocity difference at the S1 interface.

Deleted:

Deleted: 8d

5.2 River seismic lines

Figure S3a and S3b shows the seismic processing results for the single-channel data (© SGU), and their interpretation, respectively. The seismic results still show many multiples along the line, e.g. between 2000 and 3500 m distance or between 9000 and 11000 m distance. Six filled channels labelled by C (Fig. S3b) can be distinguished along the line, the larger ones up to 2000 m wide are found in the first 11000 m distance, and the smaller ones are around 1000 m wide. Only a peak of the bedrock interface (B1) is interpreted between 5500 and 6000 m distance, separating two adjacent channels. The interpretation of the areas separating adjacent channels in the rest of the cases, at distances around 2800, 8000, 11500, 13000 and 15000 m, is complicated because no more structures are clearly visible. The reasons may include the bedrock being very close to the surface and/or the presence of fracture zones as shown in the interpretation of the six-channel data.

The results of the six-channel data collection (© SGU) and their interpretation are presented in Fig. 7a and 7b, respectively. Figure 7b also includes the total sounding data from boreholes 11014, 11034 and 11094 (BGA, 2018). The difference in height between the valleys and peaks reaches up to 15 m (Fig. 7a). Although the resolution of the six-channel data compared to the single-channel data is lower, geological features can be distinguished at greater depth (>100 m). In the interpreted section (Fig. 7b) the same channels (C) identified in the single-channel data (Fig. S3b) except one can also be delineated, as well as the bedrock highs between 5500 and 6000 m distance (there is a difference of about 10 m in height between both data sets at this point, probably due to the distance between the lines). Strong variations in the borehole data coincide with the filled channel positions. The bedrock undulates and presents several fracture zones between CDPs 800 and 1000, 1350 and 1400, 2350 and 2500, and 2950 and 3000. These fracture zones coincide with fracture zones identified using the geological information provided by SGU (Fig. 2a). In Fig. 7b we can also observe that the reflection amplitude decreases between CDPs 3000 and 5402, the deeper areas being more affected. The bedrock interface (B1) may be closer to the surface at these positions, thus the low-amplitude region would represent the transparent crystalline bedrock.

Figure 8 shows a detailed section of the river seismic data (© SGU) between CDPs 1800 and 3300. The portion of side-scan sonar data (© SGU) corresponding to the profile AA' (Fig. 8b–c) is presented in Fig. 8a. Figure 8b and 8c are the interpreted sections of single- and six-channel data. Line 5–5b crosses a fracture zone. In Fig. 8a hummocks and disturbed riverbed are observed at the centre of the river bottom; these may be interpreted as landslide debris. The shade colour and the texture indicate denser and coarser deposits, respectively, compared to their surrounding materials. In Figs. 2a and 6a, at the position of line 5–5b, a landslide scar is found in the southern side of the river. In the opposite riverbank two more landslide scars are found as well as one gully flowing from the south and a tributary flowing from the southeast (Fig. 2a–b). Based on Fig. 8a, it is unclear whether the deposits at the river bottom originate from the landslides or are fluvial sediments.

6 Discussion

6.1 3D Modelling of the subsurface materials

Deleted: 4

Deleted: 9a and 9b

Deleted: Figure 9b also includes the total sounding data from boreholes 11014, 11034 and 11094 (BGA, 2018). The

Deleted: even

Deleted: 9b

Deleted: The curves for each borehole show strong increases when intersecting the filled channels, thus indicating the presence of coarse materials within the sediments. Note that most of the depressions along the bathymetric profile coincide with the channel positions. These depressions can reach up to 10 m difference in height with respect to peaks or mounds that are found between them.

Deleted: 10a

Deleted: 10b

Deleted: 10b

Deleted: 10a

Deleted: 10b

Deleted: 9b

Deleted: Along the whole line fractured or disturbed materials (F) can be identified at the shallowest sediments, and also at bedrock level.

Deleted: 10b

Deleted: 11

Deleted: 11b

Deleted: 11a

Deleted: 11b

Deleted: 11c

Deleted: 11a

Deleted: centre

Deleted: colour

Deleted: A

Deleted: can be

Deleted: (see also Fig. 2a and 6a)

Deleted: 11a

Formatted: English (UK)

Deleted: 5

Deleted: 5.1 Comparison with previous studies ... [1]

Deleted: 5

Deleted: 2

One of the main objectives of this study was to obtain the extension of the coarse-grained layer and its spatial relationship with the bedrock surface. Malehmir et al. (2013a, 2013b) have shown that the coarse-grained layer extended locally in a restricted area, but this work shows the extension of this layer to the north and south of the initial study area. The top of the coarse-grained layer and top of bedrock were picked on the processed land and river seismic lines, and elevation surfaces were interpolated using the seismic, borehole (BGA, 2018) and LiDAR data (© Lantmäteriet). Total sounding data identify top and bottom of the coarse-grained layer at many points at the site. The LiDAR data were used for fixing the elevation of the rock outcrops. The elevation surfaces for the top of the coarse-grained layer and top of bedrock (Fig. 9a and 9b) were calculated using a natural neighbour interpolation after a Delaunay triangulation of the scattered sample points was generated. The results are better constrained in the area surrounding the rock outcrop, as more seismic lines are available there. The top of bedrock is visible in all the lines, except line 4 (Malehmir et al., 2013b) and, therefore, the model of the bedrock surface in the study area is generally well constrained. The top of the coarse-grained layer is not identified in line 6, but the model gives a good overview of the layer extension, which spreads over both sides of the river. The maximum elevation for both the top of bedrock and top of the coarse-grained layer surfaces occupy the centre of the survey site, and the undulated bedrock dips down towards the river. The latter implies that more water may flow in the coarse-grained layer closer to the river. Löfroth et al. (2011) and Salas-Romero et al. (2016) show that the coarse-grained layer is thicker within the depressions, which is related to the deeper top of bedrock and sediment focusing when deposition took place. The thickness of the coarse-grained layer and the higher water flow could increase the thickness of potential quick clays in those depressions. We interpret the combination of coarse-grained layer, bedrock morphology and presence of fractured bedrock to contribute to the formation of quick clay and to be likely pre-conditioning factors for landslide (see e.g. L'Heureux et al., 2017).

Figures **S4** and S5 **show different** perspectives **of this modelling together with the 3D visualization of the seismic profiles.** In Fig. S4c, **two elongated depressions next to the river, which cross lines 2–2b, 5–5b, 6 and 7, can be identified. These depressions are interpreted as possible faults and coincide with the position of mapped fracture zones (Fig. 2a). The possible faults indicate areas more susceptible to slide, together with the slope inclination and/or increased water flow**. Figure S5b show the strong bedrock undulation between lines 6 and 7, whose reflection seismic results (Figs. S1 and S2) indicate 3D effects in the western part of the profiles due to rough topography. The reflections corresponding to the filled channels correlate with the interpolated top of the coarse-grained layer surface (Fig. S5b).

6.2 3D Hydrological modelling of the coarse-grained layer

After obtaining the elevation surface for the top of the coarse-grained layer, we modelled the elevation surface for the bottom of the layer using the RMT resistivity (Lindgren, 2014; Shan et al., 2014; Wang et al., 2016) and available borehole data (BGA, 2018; Salas-Romero et al., 2016). Thickness values of the coarse-grained layer were picked along the RMT resistivity profiles at its estimated position. The thickness of the layer was then interpolated together with thickness values obtained

Formatted: Normal, Left, Space After: 12 pt, Line spacing: at least 16 pt, No widow/orphan control, Don't adjust space between Latin and Asian text, Don't adjust space between Asian text and numbers

Deleted: horizons

Deleted: mainly

Moved down [4]: **Figure 12 shows the results of this modelling together with the 3D visualization of the seismic profiles. The bedrock surface in Fig. 12c undulates between 80.5 and -110 m elevation. Two elongated depressions next to the river, which cross lines 2–2b, 5–5b, 6 and 7, can be identified. These depressions are interpreted as possible faults and coincide with the position of fracture zones (Fig. 2a). The gentler coarse-grained layer surface in Fig. 12d ranges from 18.5 to -28.5 m elevation. The data are better constrained in the area surrounding the rock outcrop, as more seismic lines are available there. The bedrock surface is visible in all the lines, except line 4 (Malehmir et al., 2013b) and, therefore, the model of the bedrock surface in the study area is generally well constrained. The coarse-grained layer is not identified in the northwestern p** ... [2]

Deleted: **Figure 12 shows the results of this modelling tog** ... [3]

Formatted: Font:(Default) Times, Bold, Italic

Deleted: coincides with

Deleted: is

Deleted: 5

Formatted: English (US)

Deleted: The possible faults indicate areas more susceptible ... [4]

Moved (insertion) [4]

Formatted: Font:10 pt, English (UK)

Deleted: 12

Deleted: s

Deleted: the results

Deleted: The bedrock surface in Fig. 12c undulates between ... [5]

Deleted: T

Deleted:

Deleted: The gentler coarse-grained layer surface in Fig. 12 ... [6]

Deleted:

Deleted: Note

Deleted: 7

Deleted: 8

Deleted: Figure 13d shows the delineation of the coarse-gra ... [7]

Deleted: t

Deleted: (see Fig. 13b and 13d)

Formatted: Font:Not Bold

Deleted: **5**

Deleted: **3**

Deleted: 5

from the borehole data. The interpolated thickness surface was subtracted from the elevation surface of the top of the coarse-grained layer previously modelled in order to obtain the elevation surface of the bottom of the coarse-grained layer.

The typical soil sequence and groundwater system in the Göta River valley is, from top to bottom, (i) an altered clay layer with an increased transmissivity reaching potentially down to 5 m and acting as an upper aquifer, then (ii) more intact clay beds acting as an aquitard, underlain by (iii) a lower aquifer consisting in a coarser layer of sand or till, and/or weathered/fractured bedrock (Persson et al., 2011). This framework was applied to the site to interpret pore pressure measurements available at different depths for an array of sites (BGA, 2018) and water levels at the boreholes BH1 to BH3 (Table S2). The water pressure looks close to hydrostatic near the ground surface, before decreasing to a minimum above the estimated depth of the coarse-grained layer, which is found to have a higher pressure than the overlaying clays, sometimes even displaying artesian conditions (Tables S2 and S3). This would indicate that little to no groundwater recharge is occurring through the clay down to the coarse-grained layer. The pressure values in the coarse-grained layer exhibit a decreasing trend when travelling from the higher elevation outcrops in the centre of the study area down to the river (Table S2, and Fig. 10a). The central part of the model is characterized by the disappearance of the coarse-grained layer, a thin sandy-silty till cover and several elevated rock outcrops (Fig. 2a), which we hypothesize to be a groundwater recharge area for the coarse-grained layer by infiltration along the bedrock/sediments interface. The coarse-grained layer seems to be hydraulically connected to the river, at least intermittently.

To test these insights the elevation and thickness values for the coarse-grained layer were used to build a single-layer two-dimensional confined aquifer model for the coarse-grained layer (Fig. 10a), governed by the steady-state groundwater flow Eq. (1) (Bear, 1972):

$$\boldsymbol{div}\left(\boldsymbol{T}\,.\,\boldsymbol{grad}(\boldsymbol{h})\right) = \boldsymbol{0}\,, \quad (1)$$

where the hydraulic head (h) is the unknown variable. A horizontal model resolution of 10 m was chosen and the problem was solved using a finite volume method (Guyer et al., 2009). The transmissivity (T) was defined as the product of the local interpolated coarse-grained layer thickness with a uniform hydraulic conductivity (K), the latter needed to be calibrated (Fig. 10b). The transmissivity values are higher (from 0.0035 to 0.0095 m^2/s) around the land seismic lines, due to a thicker coarse-grained layer at these positions. As hydraulic boundary conditions, the cells directly underlying the river were assumed to have a fixed head corresponding to the average river level as shown in Fig. 2b. The area of the considered recharge zone (A) is approximately 0.2 km^2 and the groundwater recharge rate was used as a calibration parameter. The recharge area was represented as a fixed flux boundary condition to the adjacent coarse-grained layer cells. Consistently with the vertical pore pressure profiles, the groundwater recharge rate over the rest of the model domain (outside the recharge zone) was deemed unlikely to exceed 5 % of the normal annual mean net precipitation (Pnet) in the catchment estimated at around 460 mm/year (Swedish Meteorological and Hydrological Institute–SMHI, 2018), and was effectively set to zero.

Formatted: English (UK)

Deleted: T

Deleted: for obtaining

Deleted: groundwater

Deleted: 4

Deleted: hich reflects a gradual decrease of the hydraulic head from the outcrop area to the river

Deleted: The

Deleted: is

Deleted: . Groundwater table from the existing boreholes in the study area (see Fig. 2b and 14a) matches the groundwater level obtained in the model. Boreholes 7056, 7060 and 7069 do not fit the groundwater model, possibly due to having only one measurement of the water table, which may have fluctuated at a later stage. The total volume (V) of the interpolated coarse-grained layer was estimated around 5 hm^3. The steady-state confined groundwater flow Eq. (1) (Bear, 1972) is: ... [8]

Deleted: 4

Formatted: Not Highlight

Deleted: 6

Formatted: Not Highlight

Deleted: 16

Deleted: The central part of the model is characterized by the disappearance of the coarse-grained layer, a thin sandy-silty till cover and several elevated rock outcrops (Fig. 2a), which we hypothesized to be a groundwater recharge area for the coarse-grained layer by infiltration along the bedrock/sediments interface.

Deleted: layer of constant T, equal to 0.001 m^2/s, in order to distribute the recharge to the adjacent coarse-grained layer. After a few tests, the groundwater recharge rate over the rest of the model domain was deemed unlikely to exceed 5 %

Eight groundwater level and pore pressure values from the existing boreholes in the study area or measured near the depth of the coarse-grained layer (see Fig. 10a and Table S2) were used as targets to fit the log10 value hydraulic conductivity (log K) of the coarse-grained layer and the recharge rate over the central outcrops (expressed as a fraction f of the annual mean net precipitation). The calibration was obtained by minimizing the root-mean-square-error (RMSE) on the eight modelled pressure values following a conjugate gradient method. The model approaches the targets with a RMSE of less than 0.5 m for an effective log K value of -3.15 ± 0.15 (or K = 0.0007 m/s), which is plausible for a coarse sandy layer, and a recharge rate over the central part of the model of about 165 mm/year, which is about 36 % (± 10 %) of the normal net precipitation for this catchment (SMHI, 2018; Fig. 10d).

According to this model, the groundwater recharge through the top fine-grained sediment layers is of second order to explain the hydraulic behaviour of the coarse-grained layer. Artesian conditions can be found on low grounds near the river, sometimes only at peak flow conditions. A calculation of the water residence time (tau) in the coarse-grained layer can be done according to Eq. (2):

$$tau = \frac{V * phi}{A * Pnet * 0.36}, \quad (2)$$

which is approximately 48 years, assuming a porosity (phi) of 0.3 (or 30 %) and a calculated volume V of the coarse-grained layer of 5 hm^3. This relatively short residence time would point to lower salinity groundwater occurrences in the coarse-grained layer compared to the overlying clays and ion transfer from the clays to the underlying groundwater flow system by diffusion (Torrance, 1979) and/or by seasonal in/outflow cycles of groundwater flow between the coarse-grained layer and the overlying clays, which has been identified as a precursor to the formation of quick clays (Rankka et al., 2004). Figure 10c shows the values of the mean groundwater velocity (Darcy flow vector amplitude divided by phi) and vector field of the Darcy flow, whose directions go from the outcrop area to the river. At positions where T (or thickness of the coarse-grained) is lower (less than 0.0035 m^2/s), the mean groundwater velocity is higher (from 0.00006 to 0.00010 m/s), and vice-versa, where T is large (from 0.0035 to 0.0095 m^2/s) the velocity is very low (less than 0.00007 m/s). Assuming that the leaching of marine salts increases with groundwater velocity, areas where the groundwater velocity is higher could be at an increased risk of quick-clay formation.

6.3 Morphology of the Göta River valley

The total-field magnetic data were corrected for differences in diurnal variations and instrumental drift using the base station data (a background, International Geomagnetic Reference Field–IGRF, value of 50600 nT was subtracted from the results to convert to residual magnetic anomaly data). However, several inconsistencies were still present in the corrected data such as different values at overlapping positions, level jumps between measurement days (see sketch with the measurement and base station positions in the lower right corner in Fig. 11a), and elongated features parallel to the measuring paths. In order to level the data, a constant value was added or removed in the measurements for the last three days, and the polarity was changed for the data of the first day. For removing the elongated features, the data were divided in two groups, the first three

Deleted: G

Deleted: measurements, although sparse, indicate either large seasonal variations of the water table or sporadic connections to a deeper groundwater system via bedrock fracture zones. In the present model, the coarse-grained layer hydraulic conductivity and the recharge rate over the central outcrops were manually fitted against the groundwater head measurements in the available boreholes (measurement dates are April/May of 2010 and middle March of 2013). The model predicts an effective K of 0.001 m/s, which is plausible for a coarse sandy layer, and a recharge rate over the central part of the model of about 210 mm/year, which is about 45 % of the normal net precipitation for this catchment (SMHI, 2018).

Deleted: are not

Formatted: English (UK)

Deleted: to be prevalent under 'spring' base conditions but a shift to seasonal artesian conditions during the high-water season (from June to December) cannot be ruled out in light of the available data

Deleted: 4

Deleted: 5

Deleted: 20

Deleted: 2

Deleted: 2

Deleted: , either

Deleted: or by slow infiltration

Deleted: 4

Formatted: Not Highlight

Deleted: 6

Formatted: Not Highlight

Deleted: 5

Formatted: Not Highlight

Deleted: 5

Formatted: Not Highlight

Deleted: 6

Formatted: Not Highlight

Deleted: 162

Formatted: Not Highlight

Deleted: 12

Deleted: 5

Deleted: 4

Deleted: ,

Deleted: , Earth magnetic field,

Deleted: 5

days and the last two days of measurements, gridded and filtered similar to the micro-levelling procedure (Minty, 1991). A low-pass filter was applied in N-S direction, a high-pass filter in the E-W direction, and then the result was subtracted from the original gridded data. The final result (Fig. 11a) is smoother and more homogeneous than the initial data but still has few elongated features, which are residual errors (acquisition footprint) and not natural features as they coincide with the sampling directions.

Figure 11a shows that the residual magnetic anomaly values are higher on the northern part than on the southern (ranging from -20 to 20 nT); at the bottom and in the eastern flank of the landslide scar that crosses line 5–5b the values reach 20 nT. Almost all along line 4 and between lines 2–2b and 5–5b higher residual magnetic anomaly values are found. Salas-Romero et al. (2016) showed that the coarse-grained layer has higher magnetic susceptibility compared to the sediments above and below of these materials. Besides, we also took samples at the bottom of the landslide scar up to 1.5-2 m depth that were identified as silty-sandy. The high residual magnetic anomaly values at the landslide scar may indicate that the coarse-grained layer, which drains the water infiltrated from the nearby outcrops and/or fractures, may have acted as sliding surface together with quick clays. L'Heureux et al. (2012) identified a 'weak layer' composed of softer and more sensitive clays and sands (compared to the surrounding materials) that acted as slide prone layer in the initiation of the 1996 Finneidfjord landslide. This layer also contained biogenic gas, which may have affected its geotechnical properties. Biogenic gas was found in boreholes BH2 (Salas-Romero et al., 2016) and 7075 (BGA, 2018), which adds another similarity with the case described in L'Heureux et al. (2012). According to the farmer working these lands the landslide scar was formed approximately 50 years ago, and the landslide could have been triggered due to changes in the river water level and/or an increase in pore pressure, and/or toe erosion. Looking the borehole information available in the area (BGA, 2018; Löfroth et al., 2011; Salas-Romero et al., 2016), the top of the coarse-grained layer lies between 10 and 30 m depth, being deeper at boreholes 7206 and BH2. At the latter borehole, the thickness of the coarse-grained layer reaches almost 10 m (in BH1 and BH3 the thickness of this layer is about 1 and 3 m, respectively). The shallowest tops of the coarse-grained layer are registered at borehole 7202 at the landslide scar and at BH1. Comparing this information with the residual magnetic anomaly data, we infer that the coarse-grained layer, its distance to the surface and thickness, may be related to the high values of the magnetic data in the northern part and around BH1 where line 1 lies. The bedrock at these positions is quite deep to cause such high values (e.g. in BH2 the top of bedrock is around 78 m). The southwestern part does not reflect the same behaviour, which may be related to the thinness of the coarse-grained layer and/or its depth. On the southern part of the residual magnetic anomaly map an elongated anomaly that follows SW-NE direction is observed. The values are higher in the centre (ranging approximately between -15 and 5 nT), with the maximum values around borehole 7067 (BGA, 2018) in the intersection with line 2–2b, and lower around the anomaly (ranging from -25 to -15 nT). At borehole 7067, bedrock is close to the surface, with high residual magnetic anomaly values coinciding with the bedrock topography. We interpret the elongated anomaly to be related to the scarp formed between bedrock and the lower elevated sediments to the west (Fig. 2). The southeastern part of the residual magnetic anomaly map where there are several outcrops and the surface elevation is

Deleted: 5

Deleted: 5

Deleted: 5

Deleted: ng

Deleted: 5

Deleted: T

Deleted: according to the farmer working these lands,

Deleted: 5

Deleted: around

higher, includes negative and positive magnetic anomalies. A few houses and farms may have influenced the residual magnetic anomaly data in this area.

In order to test these how the high values of the residual magnetic anomaly relate to the thickness of and depth to the top of the coarse-grained layer, and also with the depth to the top of bedrock, the different variables have been compared for two selected areas, a northern and a southern one (see magenta boxes in Fig. 11a). The northern area includes the northern tip of the SW-NE elongated anomaly, mentioned earlier. A 3D cross-plot of the above-mentioned variables exhibits two clusters of high values of residual magnetic anomaly (Fig. 11b). The high values in one of the clusters seems to be related to large thickness of the coarse-grained layer and/or shallow depth to the top of this layer (see labelled I in Fig. 11b). The second cluster of high values is located at deeper depth to the top of coarse-grained layer and lower thickness of this layer, but instead the top of bedrock is shallower (see labelled II in Fig. 11b). Similar clustering related to the depth of the top of bedrock is observed in the southern area (Fig. 11c). Other areas more to the north have been tested and the results show a mix of trends (including residual errors), which makes interpretation difficult. This suggests that the residual magnetic anomaly data are complex, but correlate positively with the presence of the coarse-grained layer and/or bedrock.

Figure 16 presents three examples of combining the side-scan sonar (© SGU) with the bathymetric data (© SGI) on the river (see positions in Fig. 2c). The first example, Fig. 16a–e, is a section that is crossed by line 5–5b. Deposits of unclear origin can be observed at the bottom of the section (Fig. 16a); their granular texture and darker colour indicate that they may be harder and denser than the surrounding materials. These deposits may proceed from the landslide scars in both sides of the river (Fig. 2) and/or from the discharge of sediments transported by the gullies or tributary intersecting the Göta River at this position. Slopes in profile AA' can be classified as "high terrace-steep slope" (Millet, 2011), with values ranging between 30° and 45°. Profile BB' (Fig. 16d–e) shows the same type of slope on the northern riverbank, and a gentler slope (the slope is a mix between "high terrace-steep slope" and "straight uneven profile", Millet, 2011) on the opposite side. The B' extreme coincides with the position of a stream (Fig. 2). The toe of slope probably contains material due to the collapse of the subaquatic slope or sediments deposited by the stream. The second example, Fig. 16f–j, is a section located south of the study area. Profile AA' shows a possible subaquatic landslide scar in the western side. Figure 16g–h shows a "double terrace" (slopes between 40° and 55°) on the western side and a "high terrace-steep slope" (inclination around 47°) on the opposite side. The deepest terrace in the western side has a ledge that is around 5 m high, which coincides with the position of the identified subaquatic landslide scar. Profile BB' (Fig. 16i–j) shows accumulated material against the riverbank in the eastern side. The slope on the western side can be classified as a "high terrace-steep slope" (slope ~50°), and the slope profile on the opposite side resembles a combination of the classes "high terrace-steep slope" and "straight uneven profile" (maximum slope is around 30°). The toe of slope seems to consist of landslide deposits. The third example, Fig. 16k–m, is a section even more to the south than the one in Fig. 16f–j. Accumulated material is visible at the bottom of the river in the eastern side in profile AA' (Fig. 16l). The inclination of the slope is very irregular, generally below 20° but with some parts having higher inclination. The slope looks like a "straight uneven profile", although there are parts with small terraces. The

Deleted: -

Deleted: ure

Deleted: -

Deleted: ure

Deleted: -

toe of slope appears to have formed from landslide deposits. The opposite side resembles a "high terrace-steep slope" (slope is 45°).

Erosion and landslide processes have formed the landscape of the Göta River valley (SGI, 2012a). Land and river seismic data, together with side-scan sonar and bathymetric data give a good overview of the (sub-)surface in this valley. Along the river filled channels are identified, which were probably formed when the riverbed morphology changed over time. The bedrock at the river channel shows several fracture zones. The slopes of the riverbanks are generally steep and many subaquatic landslide scars and deposits can be found along the river. The origin of these deposits may also be related with the remains from the erosion protections placed between 1960 and 1970 along the Göta River. The likelihood of retrogressive landslides inland can increase due to undercutting of riverbanks during high discharge or wave erosion generated by shipping movement, which reduces lateral support and causes more instability (SGI, 2012a). At the surface, the inclination of the slopes is influenced by the land use and precipitation induced processes (SGI, 2012a).

According to SGI, our study area has, in general, medium landslide risk. Close to the river the risk is higher due to the presence of highly sensitive clays or quick clays. SGI has evaluated the risk of landslides along the Göta River under different climate change scenarios (2012a, 2012c). These scenarios estimate increases in temperature by 4-5° and 20-30 % more precipitation by 2100. High and low drainage levels from Lake Vänern will be more frequent, sea level will rise up to 0.7 m at Göteborg, and maximum groundwater levels and pore pressure in slopes will not change significantly. These conditions could increase the occurrence of landslides and modify the valley morphology in the future (SGI, 2012a). Erosion has a great impact to the south of Lilla Edet, and under these climate change scenarios will be more intense along the river's course (SGI, 2012a). This means that although the study area is located to the north of Lilla Edet, where erosion has less impact, any small change in the erosion rate in the future could cause serious effects as this area is already considered to be at medium-high landslide risk.

7 Conclusions

Through an extensive reflection seismic investigation, which includes four new land seismic profiles as well as the incorporation of existing profiles and river lines and their combination with other geophysical, geotechnical and borehole data, this study allows large-scale delineation of a coarse-grained layer, underlying bedrock and fracture zones in an area prone to quick-clay landslides in southwest Sweden. This is the first time in Sweden that land and river reflection seismic data are combined for studying the subsurface associated with this type of landslide.

Some of the geological and geohydrological prerequisites for the formation of quick clay in nature specified by Rankka et al. (2004), are shown in the results of this study. Correlation of reflection seismic, resistivity and P-wave refraction tomography results offers information about the presence of underlying coarse-grained layers, peaks in the bedrock surface, and approximated thickness and type of clay deposits. 3D subsurface morphology modelling of the coarse-grained layer and bedrock illustrates the possible infiltration points in the area, as nearby elevated rock outcrops or fractures. Hydrological

Deleted: 6

Deleted: nd

Deleted: the

Deleted: in a regional scale

Deleted: s

Deleted: the elevation surfaces for

modelling of the coarse-grained layer suggests that the dominant leaching processes are diffusion and/or seasonal in/outflow cycles of the groundwater flow between the coarse-grained layer and the overlying clays. The formation of quick clays is more significant under artesian groundwater conditions that can be found in the low elevation grounds near the river at the survey site. Ground residual magnetic anomaly data are positively correlated with the thickness and distance to the coarse-grained materials and bedrock topography. The northern part of the study area contains a shallower and thicker coarse-grained layer. At the bottleneck landslide scar present in the centre of the survey, the high residual magnetic anomaly values are most likely due to the presence of the coarse-grained layer (containing magnetic minerals), which suggests that it may have acted as sliding surface together with quick clays, similar to the 'weak layer' identified by L'Heureux et al. (2012) in Norway. The side-scan sonar and bathymetric data reveal a number of distinct morphological features in the Göta River valley that reflect the erosional processes, landslide scars and mass-movement deposits.

This work illustrates the significance of studying subsurface geology, including features within bedrock that are often overlooked when investigating landslides, especially ones that involve quick clays.

Data availability. The land reflection seismic results and modelling, magnetic results and hydrological modelling are available online with restricted access (permission from Alireza Malehmir is necessary before the data can be accessed) at https://doi.org/10.5878/acbv-h350 (Salas-Romero et al., 2019a), https://doi.org/10.5878/md19-qw71 (Salas-Romero et al., 2019b), https://doi.org/10.5878/a8xn-fc97 (Salas-Romero et al., 2019c), https://doi.org/10.5878/19t9-js25 (Salas-Romero et al., 2019d), respectively. The river reflection seismic, side-scan sonar and geological raw data are available from SGU following registration. The bathymetric raw data are available from SGI following registration, and the geotechnical data are available online at http://bga.swedgeo.se/bga/. The resistivity and tomography modelling results are properly cited and referred to in the reference list.

Author contributions. SS and AM participated in the acquisition of the land reflection seismic and magnetic data. AM designed the fieldwork campaigns of 2011 and 2013 in the study area. SS processed the land and river reflection seismic data with the support from AM. SS performed the geological modelling. SS analysed, corrected and processed the magnetic data. SS prepared the data used for the hydrological modelling, which was performed by BD. BD wrote most of the hydrological modelling section. SS made an integrated interpretation of the geophysical, geotechnical, geological and hydrological data with the help of all co-authors. SS is the main contributor to the writing of this article. All co-authors including IS contributed to the final version of this article.

Competing interests. The authors declare that they have no conflict of interest.

Deleted: estimates the size of the catchment area and
Deleted: for the low-water season (
Deleted: slow infiltration)
Deleted: , which may be dominant
Deleted: high-water season (summer and autumn)
Deleted: delineate
Deleted: indicate
Deleted: y have
Deleted: .
Deleted: ,
Deleted:
Formatted: English (UK)
Deleted: A
Deleted: A
Deleted: in
Deleted: A
Formatted: English (UK)

Acknowledgements. The GWB program of SEG and Uppsala University sponsored this project. The geophysical data were collected with the help of PhD and MSc students from Uppsala University, and staff from SGU, in particular S. Ohlsson. This study was initiated as part of a joint research collaboration among Uppsala University, SGU, Leibniz Institute for Applied Geophysics, University of Cologne, Syiah Kuala University, Polish Academy of Sciences, Norwegian Seismic Array, Norwegian Geotechnical Institute, Institute for Geosciences at the University of Oslo, Geotechnical Group at the Norwegian University of Science and Technology, and Geological Survey of Norway. Partial funding from Trust2.2-Geoinfra project (http://trust-geoinfra.se/) supported this work (252-2012-1907). We are thankful to SGU, especially to B. Bergman, and SGI for providing data. We would like to thank S. Wang, C. Shan, A. Lindgren and M. Bastani for providing their resistivity and tomography modelling results. S. Andersson helped in the processing of one of the land seismic lines as part of her MSc studies. GLOBE Claritas™ under license from GNS Science, Lower Hutt, New Zealand was used for processing the seismic data. Figures were prepared using Generic Mapping Tools (http://gmt.soest.hawaii.edu/), Inkscape (https://inkscape.org/), and Paradigm GOCAD®. Side-scan sonar, bathymetric, and magnetic data were processed and represented using MATLAB®. OpendTect (https://www.opendtect.org) and MATLAB® were used for obtaining the seismic horizons and interpolated elevation surfaces between the seismic sections. FiPy (https://www.ctcms.nist.gov/fipy) and MATLAB® were used for the hydrological modelling. We thank A. Booth, an anonymous reviewer and the topical editor for their constructive comments and suggestions that helped improve an early version of this article.

Deleted:

References

Bastani, M., Persson, L., Löfroth, H., Smith, C. A., and Schälin, D.: Analysis of ground geophysical, airborne TEM, and geotechnical data for mapping quick clays in Sweden, in: Landslides in sensitive clays, Advances in Natural and Technological Hazards Research, edited by: V. Thakur et al., Springer, Vol. 46, 463–474, https://doi.org/10.1007/978-3-319-56487-6_41, 2017.

Bear, J.: Dynamics of fluids in porous media, Dover Publications, New York, 1972.

Black, R. A., Steeples, D. W., and Miller, R. D.: Migration of shallow seismic reflection data, Geophysics, 59(3), 402–410, https://doi.org/10.1190/1.1443602, 1994.

Branschens Geotekniska Arkiv: Geosuite borrhål (och tillhörande Geosuite projektområden), Swedish Geotechnical Institute, available at: http://bga.swedgeo.se/bga/, last access: 1 March 2018.

Dahlin, T., Löfroth, H., Schälin, D., and Suer, P.: Mapping of quick clay using geoelectrical imaging and CPTU-resistivity. Near Surf. Geophys., 11(6), 695–670, https://doi.org/10.3997/1873-0604.2013044, 2013.

Demers, D., Robitaille, D., Lavoie, A., Paradis, S., Fortin, A., and Ouellet, D.: The use of LiDAR airborne data for retrogressive landslides inventory in sensitive clays, Québec, Canada. in: Landslides in sensitive clays, Advances in natural and Technological Hazards Research, edited by: V. Thakur et al., Springer, Vol. 46, 279–288, https://doi.org/10.1007/978-3-319-56487-6_25, 2017.

Gregersen, O.: The quick clay landslide in Rissa, Norway: The sliding process and discussion of failure modes, Publication No. 135, Norwegian Geotechnical Institute, Oslo, Norway, 1981.

Guyer, J. E., Wheeler, D., and Warren, J. A: FiPy: Partial Differential Equations with Python, Comput. Sci. Eng., 11(2), 6–15, https://doi.org/10.1109/MCSE.2009.52, 2009.

Hultén, C., Edstam, T., Arvidsson, O., and Nilsson, G: Geotekniska förutsättningar för ökad tappning från Vänern till Göta älv, Varia 565, Statens Geotekniska Institute, Linköping, Sweden, 2006.

Kaeser, A. J., Litts, T. L., and Tracy, T. W.: Using low-cost side-scan sonar for benthic mapping throughout the lower Flint River, Georgia, USA, River Res. Appl., 29, 634–644, https://doi.org/10.1002/rra.2556, 2013.

Larsson, S., and Jansson, M.: The landslide at Tuve, November 30 1977, Report 18, Swedish Geotechnical Institute, Linköping, Sweden, 1982.

Karlsson, R., and Hansbo, S.: Soil classification and identification, Byggforskningsrådet Document D8, Stockholm, 1989.

L'Heureux, J.-S., Longva, O., Steiner, A., Hansen, L., Vardy, M. E., Vanneste, M., Haflidason, H., Brendryen, J., Kvalstad, T. J., Forsberg, C. F., Chand, S., and Kopf, A.: Identification of weak layers and their role for the stability of slopes at Finneidfjord, northern Norway, in: Submarine mass movements and their consequences, Advances in Natural and Technological Hazards Research, edited by: Y. Yamada et al., Springer, Vol. 31, 321–330, https://doi.org/10.1007/978-94-007-2162-3_29, 2012.

L'Heureux, J.-S., Nordal, S., and Austefjord, W.: Revisiting the 1959 quick clay landslide at Sokkelvik, Norway, in: Landslides in sensitive clays, Advances in Natural and Technological Hazards Research, edited by: V. Thakur et al., Springer, Vol. 46, 395–405, https://doi.org/10.1007/978-3-319-56487-6_35, 2017.

Lilla Edets Kommun: Population in Lilla Edet, available at: https://www.lillaedet.se/, last access: 18 May 2018.

Lindgren, A.: Combined use of ground and borehole geophysical data to model spatial variations of quick clay and surrounding sediments at a Swedish landslides site, M.S. thesis, Department of Civil, Environmental and Natural Resources Engineering, Luleå University of Technology, Luleå, Sweden, 2014.

Locat, A., Locat, P., Demers, D., Leroueil, S., Robitaille, D., and Lefebvre, G.: The Saint-Jude landslide of 10 May 2010, Quebec, Canada: Investigation and characterization of the landslide and its failure mechanism, Can. Geot. J., 54(10), 1357–1374, https://doi.org/10.1139/cgj-2017-0085, 2017.

Löfroth, H., Suer, P., Dahlin, T., Leroux, V., and Schälin, D.: Quick clay mapping by resistivity–surface resistivity, CPTU-R and chemistry to complement other geotechnical sounding and sampling, GÄU-delrapport 30, Swedish Geotechnical Institute, Linköping, Sweden, 2011.

Lundberg, E., Malehmir, A., Juhlin, C., Bastani, M., and Andersson, M.: High-resolution 3D reflection seismic investigation over a quick clay landslide scar in southwest Sweden, Geophysics, 79(2), B97–B107, https://doi.org/10.1190/GEO2013-0225.1, 2014.

Lundström, K., Larsson, R., and Dahlin, T.: Mapping of quick clay formations using geotechnical and geophysical methods, Landslides, 6, 1–15, https://doi.org/10.1007/s10346-009-0144-9, 2009.

Malehmir, A., Bastani, M., Krawczyk, C. M., Gurk, M., Ismail, N., Polom, U., and Persson, L.: Geophysical assessment and geotechnical investigation of quick-clay landslides–a Swedish case study, Near Surf. Geophys., 11, 341–350, https://doi.org/10.3997/1873-0604.2013010, 2013a.

Malehmir, A., Saleem, M. U., and Bastani, M.: High-resolution reflection seismic investigations of quick clay and associated formations at a landslide scar in southwest Sweden, J. Appl. Geophys., 92, 84–102, https://doi.org/10.1016/j.jappgep.2013.02.013, 2013b.

Malehmir, A., Socco, L. V., Bastani, M., Krawczyk, C. M., Pfaffhuber, A. A., Miller, R. D., Maurer, H., Frauenfelder, R., Suto, K., Bazin, S., Merz, K., and Dahlin, T.: Near-surface geophysical characterization of areas prone to natural hazards: A review of the current and perspective on the future, in: Advances in Geophysics, edited by: L. Nielsen, Elsevier, Vol. 57, 51–146, https://doi.org/10.1016/bs.agph.2016.08.001, 2016.

Marin Miljöanalys AB: Rapport sjömätning: Göta älv, Nordre älv, U304-0909, Göteborg, Sweden, 2009.

Millet, D.: River erosion, landslides and slope development in Göta River–a study based on bathymetric data and general limit equilibrium slope stability analysis, M.S. thesis, Department of Civil and Environmental Engineering (Division of GeoEngineering), Chalmers University of Technology, Göteborg, Sweden, 2011.

Minty, B. R. S.: Simple micro-levelling for aeromagnetic data, Explor. Geophys., 22, 591–592, https://doi.org/10.1071/EG991591, 1991.

Odenstad, S.: Jordskredet i Göta den 7 juni 1957, Geologiska Föreningen i Stockholm Förhandlingar, 80(1), 76–86, https://doi.org/10.1080/11035895809447207, 1958.

Osterman, J.: Studies of the properties and formation of quick clays, Clay Clay Miner, 12(1), 87–108, 1963.

Persson, H., Bengtsson, P.-E., Lundström, K., and Karlsson, P.: Evaluation of groundwater conditions in slopes along the Göta River – General guidelines, Göta älvutredningen – delrapport 7, Swedish Geotechnical Institute, 2011.

Rankka, K., Andersson-Sköld, Y., Hultén, C., Larsson, R., Leroux, V., and Dahlin, T.: Quick clay in Sweden, Report 65, Swedish Geotechnical Institute, Linköping, Sweden, 2004.

Rosenqvist, I. T.: Om leirers kvikkaktighet, Meddelande 4, Statens Vegvesen, Veglaboratoriet, Oslo, Norway, 1946.

Rosenqvist, I. T.: Considerations on the sensitivity of Norwegian quick clays, Geotechnique, 3(5), 195–200, 1953.

Salas-Romero, S., Malehmir, A., Snowball, I., Lougheed, B. C., and Hellqvist, M.: Identifying landslide preconditions in Swedish quick clays–insights from integration of surface geophysical, core sample- and downhole property measurements, Landslides, 13(5), 905–923, https://doi.org/ 10.1007/s10346-015-0633-y, 2016.

Salas-Romero, S., Malehmir, A., Snowball, I., and Dessirier, B.: Land reflection seismic, hydrogeological and magnetic study of an area prone to quick-clay landslides in southwest Sweden, Swedish National Data Service, Version 1.0, https://doi.org/10.5878/acbv-h350, 2019a.

Salas-Romero, S., Malehmir, A., Snowball, I., and Dessirier, B.: Land reflection seismic, hydrogeological and magnetic study of an area prone to quick-clay landslides in southwest Sweden, Swedish National Data Service, Version 1.0, https://doi.org/10.5878/md19-qw71, 2019b.

Deleted: 5

Salas-Romero, S., Malehmir, A., Snowball, I., and Dessirier, B.: Land reflection seismic, hydrogeological and magnetic study of an area prone to quick-clay landslides in southwest Sweden, Swedish National Data Service, Version 1.0, https://doi.org/10.5878/a8xn-fc97, 2019c.

Salas-Romero, S., Malehmir, A., Snowball, I., and Dessirier, B.: Land reflection seismic, hydrogeological and magnetic study of an area prone to quick-clay landslides in southwest Sweden, Swedish National Data Service, Version 1.0, https://doi.org/10.5878/19t9-js25, 2019d.

Sauvin, G., Lecomte, I., Bazin, S., Hansen, L., Vanneste, M., and L'Heureux, J.-S.: On the integrated use of geophysics for quick-clay mapping: The Hvittingfoss case study, Norway, J. Appl. Geophys., 106, 1–13, https://doi.org/10.1016/j.jappgeo.2014.04.001, 2014.

Schmelzbach, C., Green, A. G., and Horstmeyer, H.: Ultra-shallow seismic reflection imaging in a region characterized by high source-generated noise, Near Surf. Geophys., 3(1), 33–46, https://doi.org/10.3997/1873-0604.2004027, 2005.

Shan, C., Bastani, M., Malehmir, A., Persson, L., and Engdahl, M.: Integrated 2D modelling and interpretation of geophysical and geotechnical data to delineate quick clays at a landslide site in southwest Sweden, Geophysics, 79(4), EN61–EN75, https://doi.org/10.1190/GEO2013-0201.1, 2014.

Solberg, I.-L., Hansen, L., Rønning, J. S., Haugen, E. D., Dalsegg, E., and Tønnesen, J. F.: Combined geophysical and geotechnical approach to ground investigations and hazard zonation of a quick clay area, mid Norway, Bull. Eng. Geol. Environ., 71(1), 119–133, https://doi.org/10.1007/s10064-011-0363-x, 2012.

Solberg, I.-L., Long, M., Baranwal, V. C., Gylland, A. S., and Rønning, J. S.: Geophysical and geotechnical studies of geology and sediment properties at a quick-clay landslide site at Esp, Trondheim, Norway, Eng. Geol., 208, 214–230, https://doi.org/10.1016/j.enggeo.2016.04.031, 2016.

Spies, B. R.: Depth of investigation in electromagnetic sounding methods, Geophysics, 54(7), 872–888, https://doi.org/10.1190/1.1442716, 1989.

Swedish Geotechnical Institute: Landslide risks in the Göta River valley in a changing climate, Final report, Part 1 - Societal consequences, Linköping, Sweden, 2012a.

Swedish Geotechnical Institute: Landslide risks in the Göta River valley in a changing climate, Final report, Part 2 - Mapping, Linköping, Sweden, 2012b.

Swedish Government Official Reports: Sweden facing climate change–threats and opportunities, Final report from the Swedish Commission on Climate and Vulnerability, SOU 2007:60, Stockholm, Sweden, 2007.

Swedish Meteorological and Hydrological Institute: Net precipitation in Sweden, available at: http://vattenwebb.smhi.se/, 2018.

Thakur, V., Degago, S. A., Oset, F., Aabøe, R., Dolva, B. K., Aunaas, K., Nyheim, T., Lyche, E., Jensen, O. A., Sæter, M. B., Robsrud, A., Viklund, M., Nigussie, D., and L'Heureux, J.-S.: Characterization of post-failure movements of landslides in soft sensitive clays, in: Landslides in sensitive clays: from geosciences to risk management, Advances in Natural and

Technological Hazards Research, edited by: J.-S. L'Heureux et al., Springer, Vol. 36, 91–103, https://doi.org/10.1007/978-94-007-7079-9_8, 2014.

Torrance, J. K.: Post-depositional changes in the pore-water chemistry of the sensitive marine clays of the Ottawa area, eastern Canada, Eng. Geol., 14, 135–147, https://doi.org/10.1016/0013-7952(79)90081-4, 1979.

Torrance, J. K.: Landslides in quick clay, Chapter 8, in: Landslides: Types, Mechanisms and Modelling, edited by: J. J. Clague and D. Stead, Cambridge University Press, 83–94, https://doi.org/10.1017/CBO9780511740367.009, 2012.

Wang, S., Malehmir, A., and Bastani, M.: Geophysical characterization of areas prone to quick-clay landslides using radio-magnetotelluric and seismic methods, Tectonophysics, 677-678, 248–260, https://doi.org/10.1016/j.tecto.2016.04.020, 2016.

Table 1. Main acquisition parameters of the seismic lines acquired in this study during March 2013.

Deleted: (

Deleted:)

	Line 2b	Line 5b	Line 6	Line 7
Survey parameters				
Acquisition System	Sercel 428 ™	Sercel 428 ™	Sercel 428 ™	Sercel 428 ™
Number of Receivers	160	324 cabled geophones, 50-1C and 24-3C MEMs planted wireless recorders	133	100
Number of Shots	157	87	129	100
Shot/ Receiver Spacing	4 m	20 m/4 m (10 m for wireless recorders)	4 m	4 m
Maximum Offset	636 m	~2300 m	528 m	396 m
Source Type	Accelerated weight drop	Dynamite (50 to 200 g)	Accelerated weight drop, sledgehammer, dynamite (50 g)	Sledgehammer, dynamite (50 g)
Recording parameters				
Record Length	10 s	10 s	10 s	10 s
Sampling Rate	0.5 ms	0.5 ms/1 ms (wireless recorders)	0.5 ms	0.5 ms
Receiver and source parameters				
Geophone Frequency	28 Hz	28 Hz, 1C-10Hz and 3C-MEMs	28 Hz	28 Hz
Number of Geophones per Set	Single	Single	Single	Single

Source Pattern	3 to 5 impacts/point	Single point/hole	5 impacts/point, single point/hole	3 to 5 impacts/point, single point/hole
Shot Depth	0 m	0.8 to 1 m	0 m, 0.9 m	0 m, 0.9 m

Table 2. Nominal resolution (Lateral, L and vertical, V) and spatial sampling (SS) of each method.

Remote sensing		Near surface geophysics		Boreholes	
Geology	L: N/A V: N/A	Land reflection seismic	L: 27-35 m V: 4-7 m	Natural gamma log	SS:0.01 m
LiDAR	L: 2 m V: 2 m	River reflection seismic	L: 4-17 m V: 0.1-2 m	Magnetic susceptibility log	SS: 0.25-0.5 m
Side-scan sonar	L: 20 cm V: N/A	Ground magnetics	SS: 0.4 m	Total sounding	SS:0.025 m
Bathymetry	L: 1 m V: 1 m				

Table 3. General range of P-wave velocities and resistivities for each identified material in the study area.

Type of material	P-wave velocity (m/s)	Resistivity (Ωm)
Silt and clays above the coarse-grained layer	400 - 1500	10 - 100
Potential quick-clays, immediately above the coarse-grained layer	–	10 - 80
Coarse-grained layer	1500 - 3000	80 - 150
Marine clays	400 - 1500	1 - 10
Bedrock	> 3000	> 100

Formatted: Font:Not Italic
Formatted: Font:Not Italic
Deleted: (
Deleted:)
Deleted: (
Deleted:)
Deleted:
Deleted: resolutions
Formatted Table
Formatted: Centered
Formatted: Centered
Formatted: Centered
Formatted: Centered
Deleted: L
Deleted: V: N/A
Formatted: Centered
Formatted: Centered
Deleted: ... [9]
Formatted: Font:9 pt
Formatted: Centered
Formatted Table
Formatted: Font:9 pt, Not Bold
Formatted: Centered
Formatted: Font:Not Bold
Formatted: Font:Not Bold
Formatted: Font:Not Bold
Formatted: Centered
Formatted: Font:Not Bold
Formatted: Font:Not Bold
Formatted: Centered
Formatted: Font:Not Bold
Formatted: Font:Not Bold
Deleted: Step ... [10]
Deleted: Step ... [11]

Figure 1. Aerial photo from the 1957 Göta landslide. The picture shows the sulfite factory located next to the river where the landslide started. A: factory, B: slide back wall and C: river. Photo: Edet group's archive.

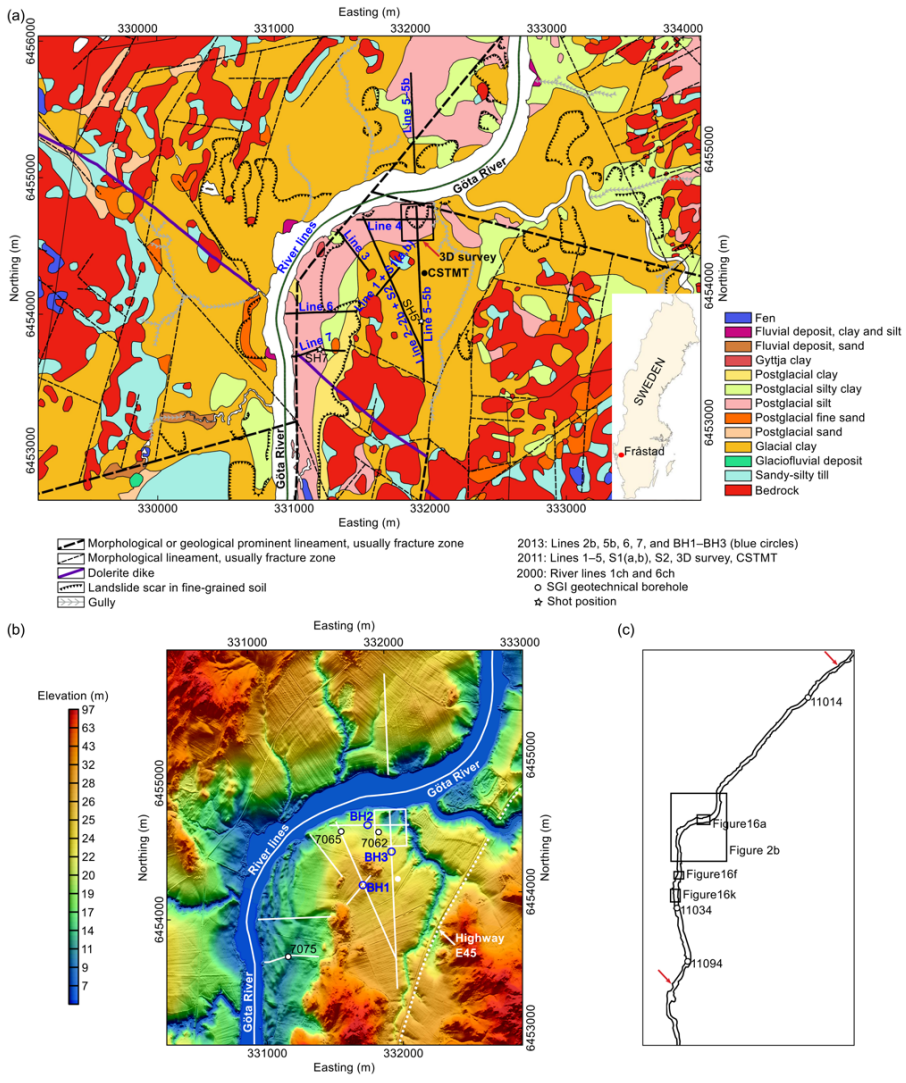

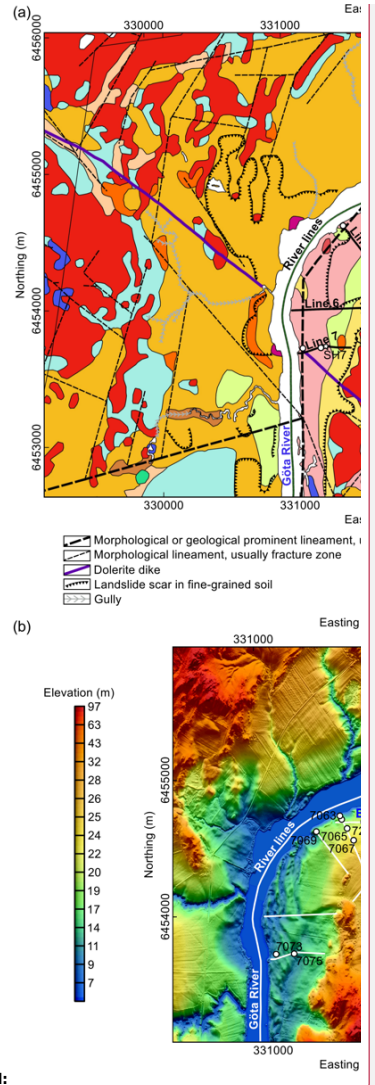

Deleted:

Formatted: Font:9 pt, Bold

Figure 2. Quick-clay study site location. **(a)** Geological map of the study area (© SGU), Fråstad, in southwest Sweden. Shot positions SH5 and SH7 (black and white stars) from line 5–5b and line 7, respectively. **(b)** LiDAR elevation map of the study area (© Lantmäteriet). **(c)** Sketch of the Göta River that includes the position of the study area (b), and the position of figures shown later in the paper. The red arrows in (c) indicate the beginning and end of the river seismic lines.

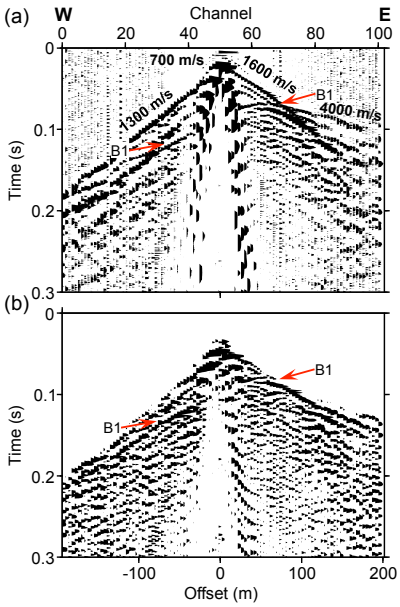

Figure 3. An example of shot record along line 7 (see SH7 in Fig. 2a). **(a)** Raw shot gather. Apparent velocities for different types of arrivals are shown at the top of each event. **(b)** The reflection B1 becomes clearer after a series of pre-stack processing steps. Scale 3H:4V.

Deleted: The legend on the right of the map shows the geological materials. The legend below the map shows the symbols for different geological structures and features, as well as some of the investigations carried out by Uppsala University, SGU and SGI.

Deleted: SGI boreholes are represented as black and white circles, and Uppsala University boreholes as blue circles. Highway E45 is visible as a straight line in the eastern part of the map.

Deleted: Fig. 2b

Deleted: in Section 5.4

Formatted: Font:Bold

Formatted: Font:Bold

Deleted: S

Deleted: (sledgehammer was used as seismic source) with trace balance applied

Deleted: A

Deleted: : elevation static corrections, Wiener deconvolution, band-pass filter, trace editing, removal of first breaks and trace balance

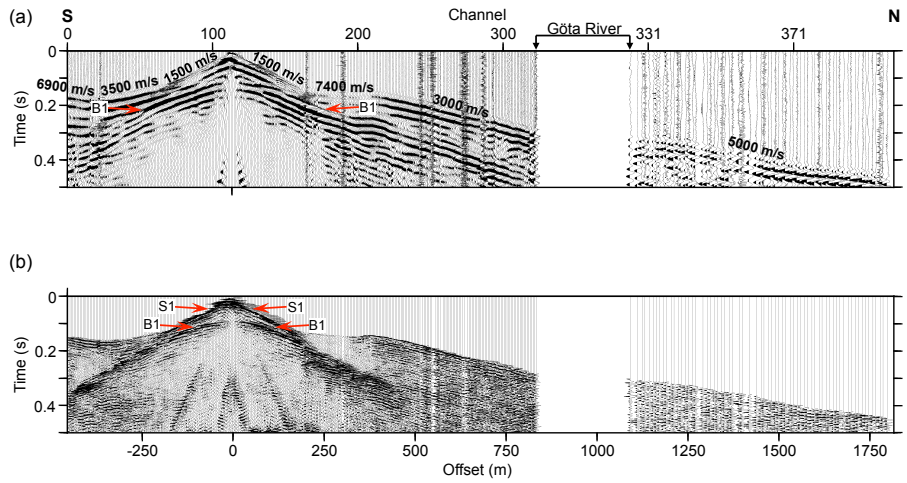

Figure 4. Shot record along line 5–5b (see SH5 in Fig. 2a). **(a)** Raw shot gather. Apparent velocities for different types of arrivals are shown at the top of each event. **(b)** Two sets of reflections seem to be revealed, B1 (top of bedrock) and S1 (top of the coarse-grained materials), after a series of pre-stack processing steps.

Deleted: (dynamite, 50 g, was used as seismic source)

Deleted: : elevation static corrections, band-pass filter, spectral whitening, trace editing, removal of first breaks and AGC.

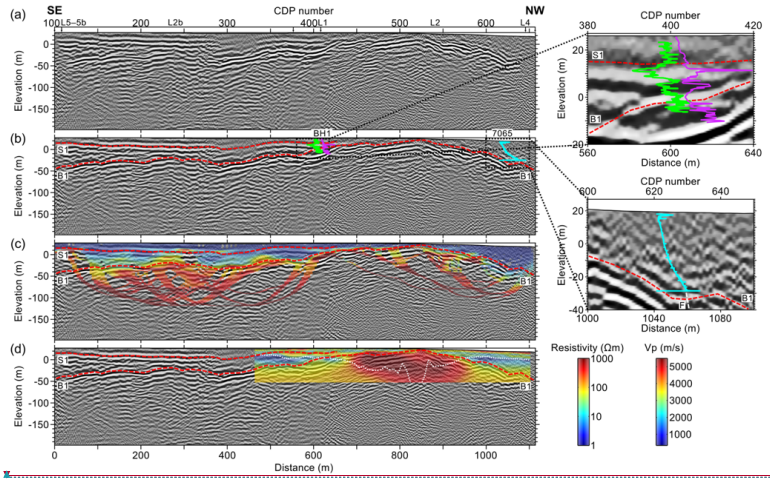

Figure 5. Merged land seismic line 2–2b. **(a)** Reflection seismic processing results. On top of the section the corresponding parts of each line and the position of the lines that intersect the merged line are indicated. **(b)** Interpreted seismic section that includes three borehole data sets, natural gamma radiation (Salas-Romero et al., 2016) in green (ranging from 87 to 182 API), and magnetic susceptibility (Salas-Romero et al., 2016) in purple (ranging from $0.09 \cdot 10^{-6}$ to $2.2 \cdot 10^{-6}$ m^3/kg) from BH1, and total sounding (BGA, 2018) from borehole 7065 in blue (ranging from 0 to 15 kN). S1: top of the coarse-grained materials and B1: top of bedrock represented by dashed red lines. **(c)** P-wave refraction tomography model (Wang et al., 2016) superimposed on the interpreted seismic section. **(d)** RMT resistivity model (Wang et al., 2016) superimposed on the interpreted seismic section. The thin dashed white line indicates the depth above which the results are considered reliable.

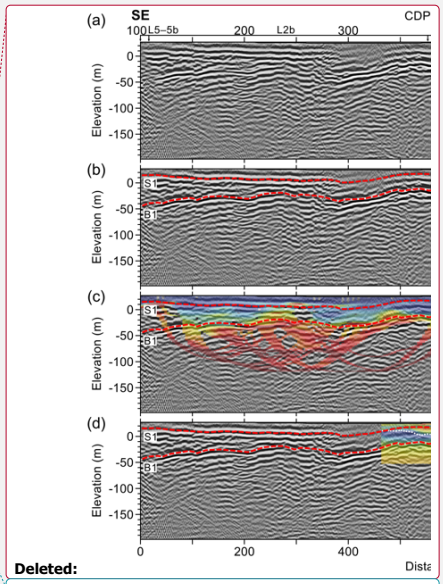

Deleted:

Formatted: Font:9 pt

Deleted: 5

Deleted: from BH1

Deleted: , distance to the seismic line 13.4 m

Deleted: 5

Deleted: from BH1

Deleted: , distance to the seismic line 0.02 m

Deleted: Close-ups for each borehole are shown on the upper right side of the figure.

Deleted: , and F: fractured or disturbed materials represented by a thick dashed white line

Deleted: .

Deleted: Resistivity and P-wave velocity values are shown in the columns located on the bottom right side of the figure.

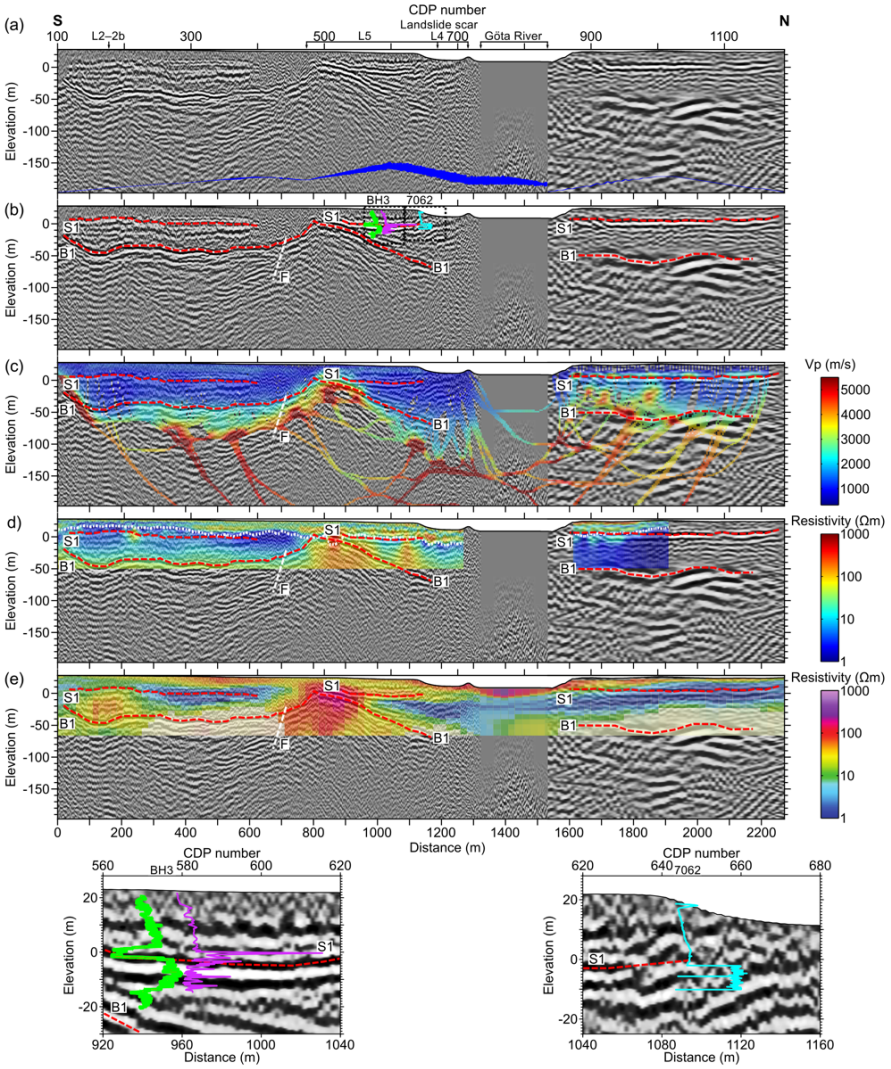
(a)
S
N
CDP number
Landslide scar
100
L2–2b
300
500
L5
L4
700
Göta River
900
1100
Elevation (m)
0
-50
-100
-150
(b)
BH3
7062
S1
B1
F
(c)
Vp (m/s)
5000
4000
3000
2000
1000
(d)
Resistivity (Ωm)
1000
100
10
1
(e)
0
200
400
600
800
1000
1200
1400
1600
1800
2000
2200
Distance (m)
560
580
600
620
20
-20
920
960
1040
640
660
680
1080
1120
1160

Figure 6. Merged land seismic line 5–5b. On top of the section the corresponding part of line 5 from 2011, the position of the lines that intersect the merged line, the landslide scar and Göta River are indicated. **(a)** Reflection seismic processing results. The fold distribution along line 5–5b is represented by a blue line at the bottom part of the section (ranging from 0 to 115). In the cabled geophone part (south) the maximum value is 115 and in the wireless part (north) 60. Note the lower fold between CDPs 400 and 480 (minimum value is 47). **(b)** Interpreted seismic section that includes three borehole data sets, natural gamma radiation (Salas-Romero et al., 2016) in green (ranging from 59 to 200 API), and magnetic susceptibility (Salas-Romero et al., 2016) in purple (ranging from $0.07 \cdot 10^{-6}$ to $2.7 \cdot 10^{-6}$ m^3/kg) from BH3, and total sounding (BGA, 2018) from borehole 7062 (ranging from 0 to 12 kN) in blue. S1: top of the coarse-grained materials and B1: top of bedrock represented by dashed red lines, and F: fractured or disturbed materials represented by a thick dashed white line. **(c)** P-wave refraction tomography model (Wang et al., 2016) superimposed on the interpreted seismic section. **(d)** RMT resistivity results (Wang et al., 2016) superimposed on the interpreted seismic section. The thin dashed white line indicates the depth above which the results are considered reliable. **(e)** ATEM resistivity results (Bastani et al., 2017) superimposed on the interpreted seismic section.

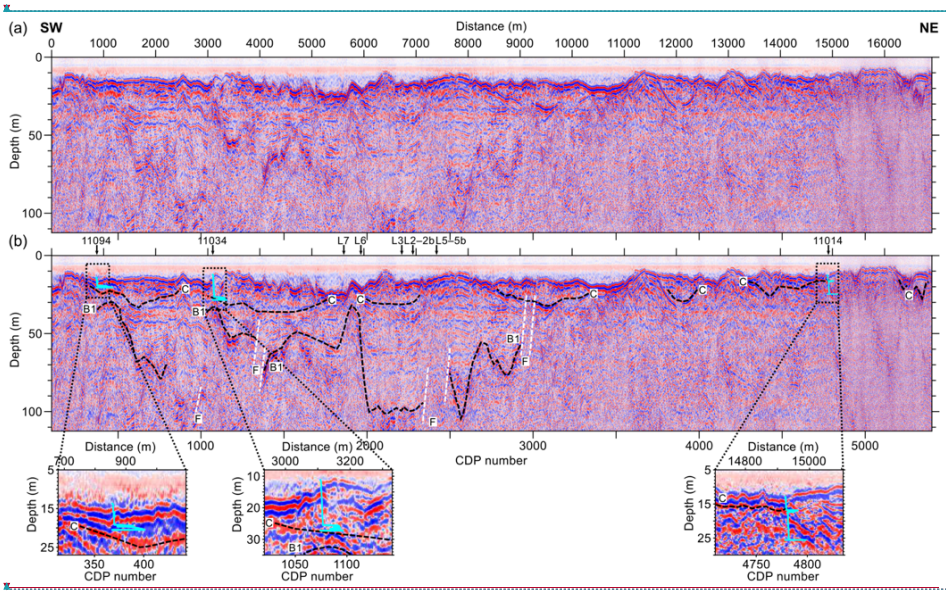

Figure 7. Processing results of the six-channel river seismic data (© SGU). **(a)** Seismic processed section. **(b)** Interpreted seismic section including total sounding data (BGA, 2018) from boreholes 11014 (ranging from 0 to 7.2 kN, distance to the line 45 m), 11034 (ranging from 0 to 9.2 kN, distance to the line 10 m), and 11094 (ranging from 0 to 11.2 kN, distance to the line 25.7 m), all in blue. C: filled channels and B1: top of bedrock represented by dashed black lines, and F: fractured or disturbed materials (no reflection continuity)

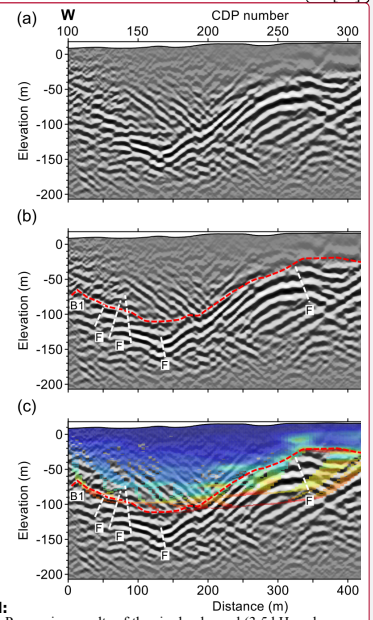

Deleted: **Figure 9.** Processing results of the single-channel (3.5 kHz echo sounder) river seismic data (© SGU). **(a)** Seismic processed section. **(b)** Interpreted seismic section including total sounding data (BGA, 2018) from boreholes 11014 (ranging from 0 to 7.2 kN, distance to the seismic line 34 m), 11034 (ranging from 0 to 9.2 kN, distance to the seismic line 20.5 m), and 11094 (ranging from 0 to 11.2 kN, distance to the seismic line 36 m), all in blue. Close-ups for each borehole are shown at the bottom part of the figure. C: filled channels and B1: bedrock represented by dashed black lines. The positions of the land seismic lines that intersect this line are indicated on top of the section. Scale 1H:57V.

Formatted

Deleted: **Figure 9.** Processing results of the single-channel (3.5 sounder) river seismic data (© SGU). **(a)** Seismic processed section. **(b)** Interpreted seismic section including total sounding data (BGA, 2018) from boreholes 11014 (ranging from 0 to 7.2 kN, distance to the seismic line 34 m), 11034 (ranging from 0 to 9.2 kN, distance to the seismic line 20.5 m), and 11094 (ranging from 0 to 11.2 kN, distance to the seismic line 36 m), all in blue. Close-ups for each borehole are shown at the bottom part of the figure. C: filled channels and B1: bedrock represented by dashed black lines. The posi

Formatted: Font:9 pt

Deleted: **10…** Processing results of the six-channel river s

represented by a dashed white line. The positions of the land seismic lines that intersect this line are indicated on top of the section. Scale 1H:30V.

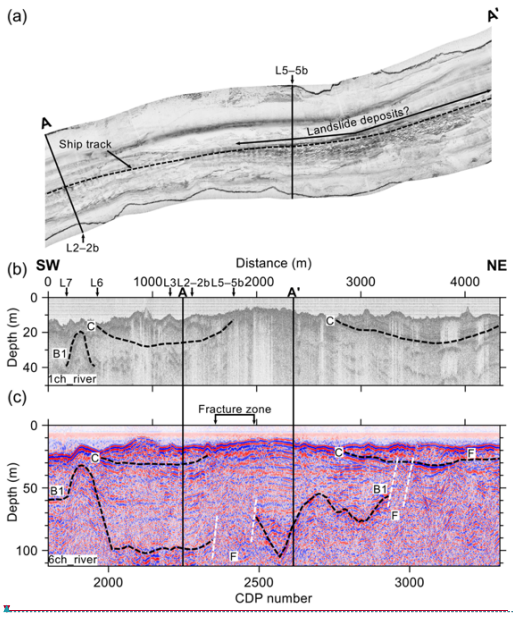

Figure 8 A section of the river seismic lines and side-scan sonar data (© SGU). **(a)** Side-scan sonar data corresponding to the profile AA' shown on top of the section in **(b)**. The land seismic lines that intersect this area are indicated. **(b)** Interpreted single-channel seismic section. Scale 1H:12V. **(c)** Interpreted six-channel seismic section. Scale 1H:12V. The positions of the land seismic lines that intersect the lines are indicated on top of **(b)**. C: filled channels, B1: top of bedrock, F: fractured or disturbed materials (no reflection continuity).

Deleted:

Formatted: Font:9 pt

Deleted: 11

Formatted: Font:Bold

Deleted: Figure 11

Deleted: track followed by the ship, the position of the possible landslide deposits and the

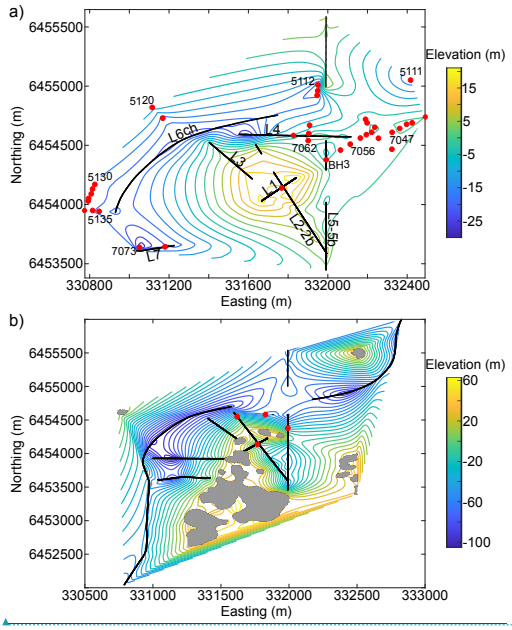

Figure 9. Elevation contours for the interpolated surfaces of **(a)** the top of the coarse-grained layer (contour spacing 3 m), and **(b)** the top of bedrock (contour spacing 6 m). The data used for the interpolation are: picked points along the seismic lines for each interface (black lines), the borehole data (red dots), and LiDAR data for the rock outcrops (grey areas). Note that only selected boreholes are labelled, but all indicated boreholes were used for the interpolation (most of the borehole data can be found in BGA, 2018).

Formatted: Font:9 pt

Formatted: Not Highlight

Formatted: Not Highlight

Formatted: Not Highlight

Formatted: Font:Not Bold

Formatted: Not Highlight

Formatted: Not Highlight

Formatted: Not Highlight

Formatted: Not Highlight

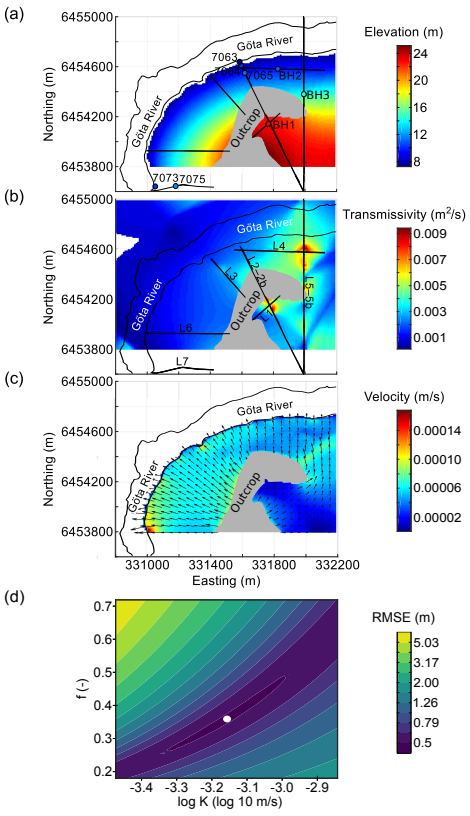

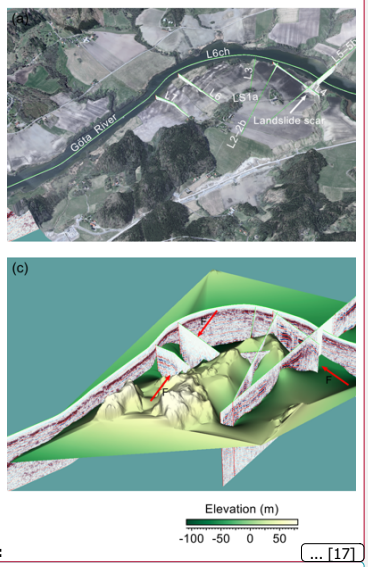

Figure 10. Hydrological modelling of a selected region in the study area. **(a)** Water table elevation. **(b)** Transmissivity distribution. **(c)** Mean groundwater velocity distribution and vector field of the Darcy flow. The position of the Göta River, outcrop area, land seismic lines (Malehmir et al., 2013a, 2013b; Salas-Romero et al., 2016) and boreholes (BGA, 2018; Salas-Romero et al., 2016) used in the modelling are indicated in the figure. **(d)** RMSE distribution. The white circle indicates where RMSE is minimum and equal to 0.5 (log K is about -3.15 and the groundwater recharge over the recharge zone is about 36 % of the normal net precipitation for this area).

Deleted: ... [17]

Formatted: Font:9 pt

Formatted: Font:9 pt

Formatted: Font:9 pt

Deleted: 4

Deleted: Range of values on the right side of each figure.

Deleted: 5

Formatted: Not Highlight

Deleted: 5

Formatted: Not Highlight

Formatted: Font:Bold, Not Highlight

Formatted: Not Highlight

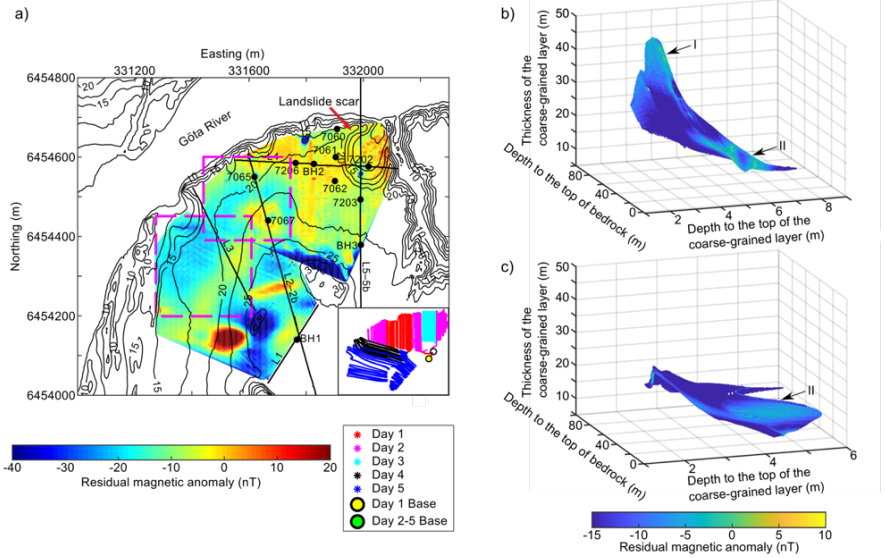

Figure 11. Residual magnetic anomaly data as **(a)** map view over the LiDAR elevation contour plot (© Lantmäteriet). **(b)** cross-plot with depth to the top of bedrock and the top of the coarse-grained layer, and the thickness of the latter for the northern area (top magenta box in **(a)**), and **(c)** cross-plot with the same variables for the southern area (bottom magenta box in **(a)**). The position of the land seismic lines (Malehmir et al., 2013a, 2013b; Salas-Romero et al., 2016) and boreholes (BGA, 2018; Löfroth et al., 2011; Salas-Romero et al., 2016) used for analysing the magnetic data as well as a sketch of the measurement and base station positions for each day are shown in **(a)**.

Deleted:
Formatted: Font:9 pt
Deleted: 5
Formatted: Font:Bold
Deleted: plotted on the contour
Deleted: of
Deleted: data
Formatted: Font:Bold
Formatted: Font:Bold
Formatted: Font:Bold
Formatted: Font:Not Bold
Formatted: Font:Bold
Formatted: Not Highlight
Deleted: 5
Deleted: 5
Formatted: Not Highlight
Deleted: the
Deleted: map
Deleted: In the bottom right, a sketch showing the measurement and base station positions for each day can be found.

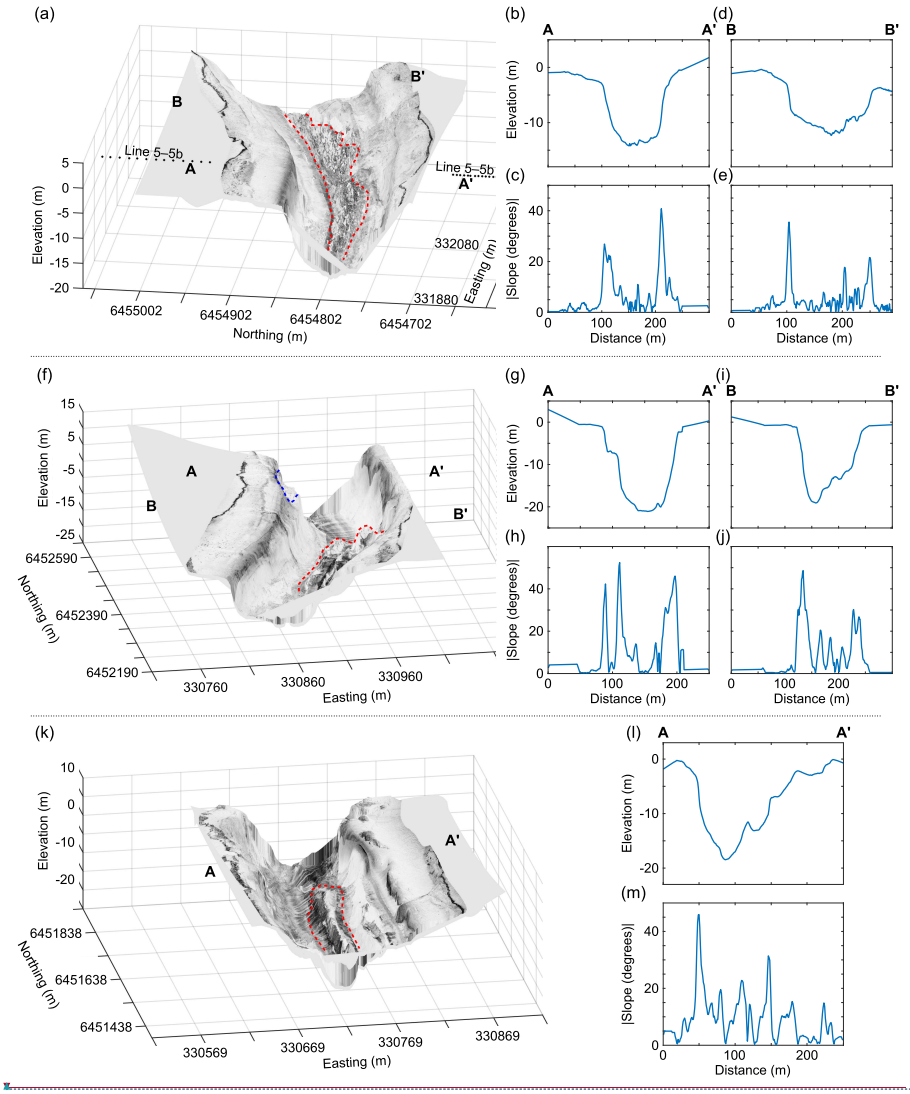

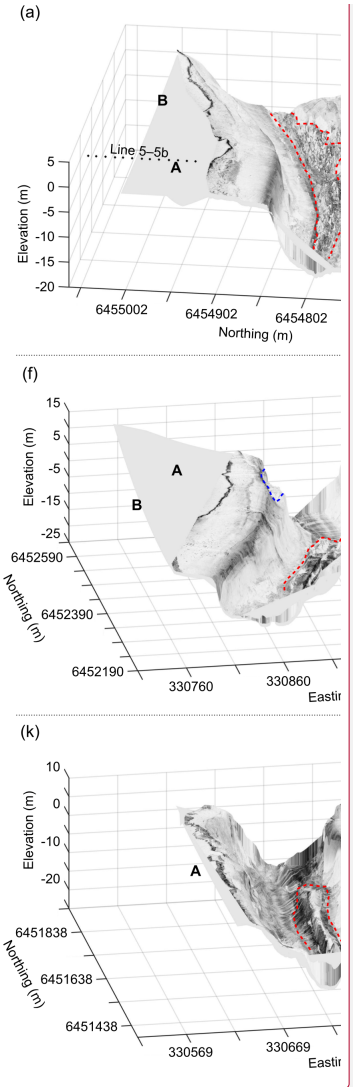

Deleted:

Formatted: Font:9 pt

Figure 12. Side-scan sonar data (© SGU) overlying the bathymetric data (© SGI) on selected segments of the Göta River. See position of the figures in Fig. 2c. **(a)** **(f)** **(k)** Cross sections of the river. Scale 1H:8V, 1H:3V, and 1H:4V, respectively. The area delineated with a dashed red line shows accumulated material at the bottom of the river and in the margins, and the dashed blue line delineates a probable subaquatic landslide scar. **(b)** **(d)** **(g)** **(i)** **(l)** Elevation along profiles AA' and BB'. **(c)** **(e)** **(h)** **(j)** **(m)** Slope (absolute values) along profiles AA' and BB'.

Deleted: 6

Deleted: next to the study area, showing also the position of line 5–5b.

Deleted: **(d)** Elevation along profile BB'. **(e)** Slope (absolute values) along profile BB'. **(f)** Cross section of the river. Scale 1H:3V. The area delineated with a dashed red line shows accumulated material in the eastern margin. The area delineated with a dashed blue line shows a probable subaquatic landslide scar. **(g)** Elevation along profile AA'. **(h)** Slope (absolute values) along profile AA'. **(i)** Elevation along profile BB'. **(j)** Slope (absolute values) along profile BB'. **(k)** Cross section of the river. Scale 1H:4V. The area delineated with a dashed red line shows accumulated material at the bottom of the river. **(l)** Elevation along profile AA'. **(m)** Slope (absolute values) along profile AA'.